Chapter 5

A Redox Role for the [4Fe4S] Cluster of Yeast DNA Polymerase δ

Adapted from: Bartels, P.L.; Stodola, J.L.; Burgers, P.M.J.; Barton, J.K. A Redox Role for the [4Fe4S] Cluster of Yeast DNA Polymerase δ. *J. Am. Chem. Soc.*, **2017**, *139*, 18339 – 18348.

P. Bartels synthesized DNA, carried out all electrochemical and spectroscopic characterization, and ran and analyzed activity assays. J. Stodola and P. Burgers provided purified proteins for experiments.

Introduction

During genomic replication, eukaryotic cells divide the task of DNA synthesis between three B-family DNA polymerases (Pols): Pol α, Pol δ, and Pol ε (*1*). In the most widely accepted model, the DNA primase-Pol α complex initiates 5′-3′ DNA synthesis by forming an RNA-DNA hybrid primer that is then extended by Pol ε on the continuously generated leading strand and by Pol δ on the discontinuously formed lagging strand (*2*). Additional roles for Pol δ during leading strand replication have been suggested (*3, 4*), and Pol δ is also involved in various DNA recombinatorial and repair processes (*5*). Structurally, each of the B-family polymerases forms a multi-subunit complex composed of a catalytic subunit and a B-subunit, with additional accessory subunits present in Pol δ and Pol ε (*6*). Recent work has shown that a $[4Fe4S]^{2+}$ cluster in the C-terminal domain (CTD) of the catalytic subunit is essential for the formation of multi-subunit complexes at least in the case of Pol δ (*6*).

While the C-terminal [4Fe4S] cluster is certainly important for complex formation (*6*), several lines of evidence suggest a more direct functional role. First, a 2.5 Å X-ray crystal structure of the yeast Pol α CTD in complex with its B-subunit contained zinc in place of a cluster, demonstrating that complex formation can be supported by simpler metals (*8*). Given the metabolic expense of [4Fe4S] cluster biosynthesis and loading into target proteins, the strict conservation of this cofactor in the B-family polymerases suggests that it serves an important function (*9*). Indeed, the importance of [4Fe4S] clusters in these enzymes is emphasized by the presence of an additional cluster in the unique Pol ε N-terminal domain (*10*).

The [4Fe4S] clusters perform a wide range of roles in biology including enzymatic catalysis and electron transfer (*11*). In the DNA polymerases, the cluster is not required for catalysis (*3, 12*). Many DNA-processing enzymes have now been shown to contain [4Fe4S]

clusters, and, in many cases, a DNA-bound redox activity of the cluster has been demonstrated (*13-16*). These diverse proteins include base excision repair glycosylases, repair helicases, and DNA primase. As in the Pol δ holoenzyme, the clusters are largely redox-inert in the absence of DNA (*17-20*). However, when bound to DNA, these protein cofactors undergo a significant negative shift in redox potential, activating the clusters toward oxidation (*21-23*). Electrochemical experiments with DNA-bound proteins show a reversible redox signal with potentials ranging from 65-95 mV versus the normal hydrogen electrode (NHE) (*13-16*). EPR studies support the assignment of the reversible signal to the $[4Fe4S]^{3+/2+}$ couple favored by high-potential iron proteins (HiPIP) that are electron carriers (*13, 24-25*). In addition to modulating redox potential, the π-stacked base pairs of DNA can act as a medium for long-range charge transport between redox-active proteins (*26*). DNA-mediated charge transport (DNA CT) is characterized by a shallow distance dependence and high sensitivity to base pair stacking, making it an excellent reporter of DNA integrity (*26*). Importantly, although DNA CT can be attenuated by proteins that bend the duplex or flip out bases, DNA CT can proceed unimpeded through nucleosome-wrapped DNA (*26*).

The redox activity of the [4Fe4S] cluster appears to be utilized in many of these proteins as a switch to regulate DNA binding and therefore activity. For the DNA repair enzyme, Endonuclease III (EndoIII), the negative shift in redox potential associated with DNA binding has been shown to lead to a 500-fold increase in DNA affinity for the oxidized $[4Fe4S]^{3+}$ cluster versus the reduced 2+ form (*27*). In the case of human DNA primase, the oxidation state of the [4Fe4S] cluster also controls template binding, and redox switching through electron transfer between clusters in primase and Pol α has been proposed to regulate RNA primer handoff (*16*).

Here we focus on Pol δ, a central B-family polymerase. We utilize a combination of electrochemical, spectroscopic, and biochemical techniques to investigate redox activity in this enzyme and to understand the consequences of redox switching for polymerase activity. These studies provide a new perspective on polymerase regulation under oxidative stress.

Materials and Methods

Protein Expression and Purification

Yeast Pol δ (WT and exo$^-$ D520V), RFC, RPA, PCNA, and *E. coli* EndoIII were expressed according to previously published protocols (*7*, *28*).

DNA Preparation

The DNA substrate for electrochemistry consisted of a 49:58-mer primer-template composed of three oligomers: a 20-mer with a 3′ thiol modification, a 38-mer, and a 49-mer complement; sequences are as follows (see also Figure 5.1c):

20-mer Thiol: 5′ - GCT GTC GTA CAG CTC AAT GC - 3′ - $(CH_2)_2O(CH_2)_3SH$

38-mer: 5′ - TAA CAG GTT GAT GCA TCG CGC TTC GGT GCT GCG TGT CT - 3′

49-mer: 5′ - GCA TT**G** AGC TGT ACG ACA GCA GAC ACG CAG CAC CGA AGC GCG ATG CAT C - 3′

The bold G of the 49-mer was changed to an A or an abasic (AP) site for CA mismatch and abasic site discrimination experiments.

Thiol-modified DNA sequences for electrochemistry were prepared by standard phosphoramidite chemistry on a DNA synthesizer (Applied Biosystems) using A, G, C, T phosphoramidites and the 3′-Thiol-Modifier 6-S-S CPG as purchased from Glen research. DNA substrates were cleaved and deprotected by 8-hour incubation in NH_4OH (Sigma-Aldrich) at 65 °C. Deprotected DNA was separated from truncation products by reverse-phase HPLC (Agilent PLRPS column, gradient of 5 – 75% ACN/95 - 25% 50 mM NH_4Ac over 30 minutes at a 2 mL/min flow rate). Thiol-modified DNA was reduced by dissolving in 50 μL Tris, pH 8.0 (Qiagen elution buffer), adding excess DTT (Sigma-Aldrich), and shaking for 45 minutes. DTT was removed by filtration through a NAP-5 column (GE Healthcare) prior to a final round of

HPLC purification (gradient of 5 – 15% ACN/95 – 85% 50 mM NH_4Ac over 35 minutes at 2 mL/min). Lastly, single-stranded DNA was desalted by standard ethanol precipitation (100 µl water, 1 mL 100% EtOH, 130 mM NaCl) and the identity of the substrate was confirmed by MALDI-TOF. Unmodified oligomers were ordered from IDT and purified by the DMT-free HPLC method. Desalted DNA was dissolved in a phosphate storage buffer (5 mM sodium phosphate, 50 mM NaCl, pH 7.0) and concentrations were determined by UV-visible spectroscopy using ε_{260} values estimated by Integrated DNA Technologies (IDT). Equimolar concentrations of single stranded DNA were then degassed and annealed (rapid heating to 95^{o} C, 5-minute incubation, and 1.5 hour cooling to 20^{o} C).

DNA replication assays used single-stranded M13mp18 plasmid purchased from New England Biolabs (NEB). Primers were purchased from IDT and purified by HPLC as described above. Primed DNA was formed by heating a 1:1 plasmid/primer mix in activity buffer (50 mM Tris-HCl, pH 7.8, 50 mM NaCl) to 90° C for 5′ and cooling to RT over several hours. The M13mp18 DNA primer had the following sequence (complementary to positions 6265-6235):

5′ - GAC TCT AGA GGA TCC CCG GGT ACC GAG CTC G - 3′

Primers were radiolabeled by incubating 10 pmol of 31-mer M13mp18 primer with T4 polynucleotide kinase (PNK) and [γ-^{32}P] ATP (Perkin Elmer) in T4 buffer (NEB) for 15 minutes at 37° C. Reactions were stopped by addition of EDTA to 10 mM and heating at 75^{o} C for 10 minutes. 2 log DNA ladder (NEB) was dephosphorylated by calf intestinal alkaline phosphatase (CIAP; 60 minutes, 37° C) prior to labeling in the same manner. As an additional size standard, duplexed M13mp18 DNA was linearized by digestion with HincII (60 minutes, 37° C) and dephosphorylated by CIAP prior to radiolabeling. Proteins and unincorporated ATP were removed using spin columns (BioRad Microspin6) equilibrated in Pol δ activity buffer (50 mM

Tris-HCl, pH 7.8, 50 mM NaCl). T4 PNK, CIAP, HincII, and dsM13mp18 DNA were purchased from NEB.

Preparation of DNA-Modified Gold Electrodes

Multiplexed chips containing 16 Au electrodes (0.015 cm^2 area) were prepared as described previously (*29*). Self-assembled monolayers (SAMs) were formed by incubating 25 μL of 25 μM duplexed DNA on the electrode overnight, after which electrodes were rinsed 3-5 times in phosphate buffer (5 mM sodium phosphate, pH 7.5, 50 mM NaCl) and backfilled for 45 minutes with 1 mM 6-mercapto-1-hexanol (Sigma-Aldrich) in the same buffer containing 5% (v/v) glycerol. Electrodes were then extensively rinsed in phosphate buffer followed by protein storage buffer (30 mM HEPES, pH 7.4, 350 mM NaAc, 1 mM DTT, 0.1 mM EDTA, 10% glycerol, and 0.01% decaethylene glycol monododecyl ether). Lastly, the absence of electroactive impurities was confirmed by scanning the surface with cyclic voltammetry (CV). Bulk electrolysis experiments were undertaken by droplet electrochemistry (30-40 μL solution) on Au rod electrodes of 0.0314 cm^2 electrode area (Pine Research Instrumentation). Electrodes were cleaned as previously described (*30*), and monolayers formed using the same procedure as the multiplexed chip.

Pol δ Electrochemistry

All electrochemical experiments were performed using a potentiostat equipped with a multiplexer, both from CH Instruments. Experiments used a standard 3-electrode cell composed of an Au working electrode, a Ag/AgCl reference electrode in 3 M NaCl (BASInc), and a 1 mm diameter Pt wire counter electrode (Lesker). Potentials were converted from Ag/AgCl to NHE by adding 212 mV to the potential as measured by Ag/AgCl; this correction accounted for both ambient temperature and the use of 3 M NaCl for reference storage (*31*). Experiments with Pol δ

were all run in polymerase storage buffer (30 mM HEPES, pH 7.4, 350 mM NaAc, 1 mM DTT, 0.1 mM EDTA, 10% glycerol v/v, and 0.01% w/v decaethylene glycol monododecyl ether).

Because PCNA can slide directly onto DNA with open ends, the clamp loader complex RFC was excluded from these experiments (*32*). WT Pol δ 3′-5′ exonuclease activity was prevented by excluding Mg^{2+} from the buffer. In initial experiments, 3-5 μM WT Pol δ or exonuclease-deficient Pol δ D520V (DV) (*33*) was incubated on the electrode for several hours in the presence of 5-10 μM PCNA. To spare enzyme, later experiments used Pol δ DV at 500 nM in combination with 5.0 μM PCNA, 80 μM dATP and 8 mM $MgAc_2$. Cyclic voltammetry (CV; 100 mV/s scan rate) and square wave voltammetry (SQWV; 15 Hz frequency, 25 mV amplitude) scans were taken once per hour for several hours. Between scans, electrodes were covered in Parafilm and stored in a humid environment to minimize evaporation. CV scan rate dependence was assessed after 3 hours using rates of 20, 50, 80, 100, 200, 500, 750, and 1000 mV/s. In experiments with abasic and CA mismatch DNA, signal attenuation was calculated as follows: [1 – ((peak area on abasic or CA mismatch DNA)/(peak area on unmodified DNA))]*100%

Pol δ concentrations are reported as the concentration of [4Fe4S] cluster, determined by UV-visible absorbance at 400 nm (ε_{400} = 13000 $M^{-1}cm^{-1}$) (*7*). The [4Fe4S] cluster loading was in the range of 70-85%, determined by dividing [4Fe4S] concentration by total protein concentration as measured by Bradford assay, Pierce BCA assay, and UV-visible absorbance at 280 nm (ε_{280} = 194100 $M^{-1}cm^{-1}$; estimated using the EXPasy ProtParam tool). Bradford and BCA assay standard curves were generated using a BSA standard, and both kits were purchased from Thermo Scientific. UV-visible spectra were taken on a Cary Varian instrument using 100 μL quartz cuvettes purchased from STARNA Cells.

When possible, diffusion coefficients were obtained from the scan rate dependence of the CV current using the Randles-Sevcik equation (*34*):

$$I_p = [0.4463(F^3/RT)^{1/2}](n^{3/2})(A)(D^{1/2})(C^\circ)\nu^{1/2} \qquad (2)$$

I_p is the peak current in amperes, F is Faraday's constant (96485 $C \cdot mol^{-1}$), R is the universal gas constant (8.314 $J \cdot (mol \cdot K)^{-1}$), T is temperature in K, n is the number of electrons transferred per CV peak, A is electrode area in cm^2, D is the diffusion coefficient in $cm^2 \cdot s^{-1}$, C° is bulk protein concentration in $mol \cdot cm^{-3}$, and ν is the scan rate in $V \cdot s^{-1}$. Experimental values of D were compared to those estimated by the Stokes-Einstein equation,

$$D = k_B T/6\pi\eta R \qquad (3)$$

where k_B is Boltzmann's constant (1.38 x 10^{-23} $J \cdot K^{-1}$), T is the incubation temperature (293 K), η is the solution viscosity (estimated to be 1.38 x 10^{-3} Pa·s for an aqueous solution with 10% glycerol), and R is the hydrodynamic radius. R was estimated to be ~26 Å from dimensions obtained from X-ray crystal structures of DNA-bound Pol3, Pol1-Pol12, and PCNA (PDB ID 3IAY, 3FLO, and 4YHR, respectively).

Electrochemical Oxidation and Spectroscopic Analysis of Pol δ

To prevent cluster degradation in the presence of O_2, bulk electrolysis was performed in an anaerobic glove bag (COY) under a 95% N_2, 5% H_2 atmosphere with an O_2-scavenging catalyst present. Buffers were degassed by bubbling in argon for several hours and stored open in the glove bag overnight prior to experiments. For spectroscopic characterization, a 150 μL sample of 1-2 μM Pol δ was added to two identical DNA-modified electrodes. On one electrode, a potential of 0.412 V vs NHE was applied for ~15 minutes, while no potential was applied to the other. Oxidation yields were estimated by taking the difference between the total charge obtained in the presence of Pol δ and that generated by electrolysis with buffer alone. Following

electrolysis, UV-visible and electron paramagnetic resonance (EPR) spectroscopy were used to confirm the integrity of the cluster after electrolysis. Samples were sealed in cuvettes for UV-visible spectroscopy, and subsequently returned to the glove bag and added to EPR tubes. Tubes were sealed by Parafilm and frozen in liquid nitrogen outside the bag. Continuous wave X-band EPR was performed at 10 K, and each experiment consisted of 9 sweeps taken at 12.88 mW microwave power, 2 G modulation amplitude, and 5.02 $x10^3$ receiver gain.

Pol δ Activity Assays

Immediately prior to assays, Pol δ DV was oxidized on Au rod electrodes exactly as described for spectroscopic characterization, but the sample was diluted to 190 nM in degassed storage buffer in a total volume of 30-40 μL. Reduction of oxidized sample was carried out at a potential of -0.188 V vs NHE for a similar length of time. In parallel with electrolysis, 140 μL reaction mixes (0.1mg/mL BSA, 80 μM each dNTP, 500 μM ATP, 2.0 nM M13mp18 with a ^{32}P-labeled primer, 8.0 mM $MgAc_2$, 500 nM RPA, 5.0 nM RFC and 5.0 nM PCNA, 50 mM NaCl, 50 mM Tris-HCl, pH 7.8) were prepared inside the glove bag. The PCNA sliding clamp was loaded onto the primer end by incubating the reaction mix with the RFC clamp loader and ATP for 1 minute at 30 °C. After clamp loading, reactions were initiated by the addition of 2 nM (final concentration) oxidized, untreated, or re-reduced Pol δ DV. Reactions were run at 30 °C, and 20 μL aliquots were removed and quenched at specific time points by adding 10 μL stop mix (10 mM EDTA and 0.1% v/v SDS final concentration). The polymerase was heat-inactivated for 10-20 minutes (55 °C), and samples were counted on a liquid scintillation counter to determine exposure time (1 hour per 300,000 counts). Samples were dried on a speed vacuum and dissolved in alkaline gel buffer (500 mM NaOH, 10 mM EDTA) with 1x alkaline loading dye (6x stock: 300 mM NaOH, 6.0 mM EDTA, 18% Ficoll w/v, 0.25% xylene cyanol w/v, and

0.15% bromocresol green w/v), and equivalent amounts of radioactivity were then loaded onto a 1% alkaline agarose gel and run at 30 V for 14-15 hours. Gels were neutralized in 7% TCA (w/v) in water for 30 minutes at RT and dried under mild pressure for several hours, exposed on a phosphor screen and visualized on a Typhoon phosphorimager (GE Healthcare). Products were analyzed using ImageQuant software (GE Healthcare). The relative amounts of DNA synthesis were determined by dividing the volume of the largest band in an oxidized sample by the equivalent band in the appropriate untreated sample.

To limit DNA synthesis to that of a single processive cycle by the PCNA-Pol δ complex, 0.01 mg/mL heparin was included in reactions (*35*) that were then analyzed on 5% polyacrylamide gels. In these instances, Pol δ was added after clamp loading and reactions were started by adding a mix of dNTPs and heparin. Quenched reactions were then counted, dried, and redissolved in 2.0 μL formamide loading dye. Immediately prior to gel loading, samples were heated at 90 ℃ for 10 minutes, and gels were run at ~50 W for 5 hours in 1x TBE buffer. Polyacrylamide gels were then exposed and imaged by phosphorimager analysis.

Tris-HCl, NaCl, $MgAc_2$, BSA, and heparin were purchased from Sigma-Aldrich, while dNTPs and ATP were from NEB. dNTPs, ATP, and $MgAc_2$ were thoroughly degassed prior to reaction, and the protein stocks were kept open during a series of vacuum/nitrogen/gas mix purges to minimize residual oxygen.

Chemical Oxidation of Pol δ

For photooxidation, the 31-mer M13mp18 primer was covalently modified with a 5′ anthraquinone (AQ). AQ was prepared as a phosphoramidite and added to the unmodified DNA on a DNA synthesizer according to previously reported procedures (*36*). The presence of AQ was verified by MALDI-TOF, and the modified primer was annealed to M13mp18 DNA in Pol δ

activity buffer (50 mM Tris-HCl, pH 7.8, 50 mM NaCl). Because the 5′ AQ modification prevented ^{32}P end-labeling, DNA was labeled by adding 2 μCi [α-^{32}P] dATP (Perkin Elmer) to the reaction, and incorporation of [α-^{32}P] dATP was facilitated by lowering the concentration of cold dATP from 80 μM to 10 μM.

Anaerobic reaction mixes lacking dNTPs were prepared in glass vials and incubated under a solar simulator equipped with a UVB/C long pass filter or in the dark for 30 minutes. To ensure complete oxidation, 2-fold molar excess of both PCNA and Pol δ DV were included. As controls, reactions were also run using unmodified DNA (no AQ) and AQ reactions were repeated with 140 nM Klenow fragment exo$^-$ (NEB). After treatment, samples were returned to the glove bag and transferred into Eppendorf tubes containing dNTPs to start the reaction. Free dNTPs were removed using BioRad Microspin 6 columns in SCC buffer (GE Healthcare) and sample radioactivity was quantified on a liquid scintillation counter. Samples were then run out on a 1% alkaline agarose gel and visualized by phosphorimaging analysis. Overall [α-^{32}P] dATP incorporation was used to compare overall DNA synthesis levels by dividing the total radioactivity counts in oxidized samples by those of dark controls.

Results

Electrochemical Characterization of Pol δ

To determine whether Pol δ holoenzyme was redox active in the presence of DNA, we carried out electrochemistry on DNA-modified gold electrodes. In initial experiments, 3 μM WT Pol δ in storage buffer was combined with 10 μM PCNA and incubated on the electrode for several hours. CV scans taken hourly reveal a reversible signal with a midpoint potential of 116 ± 3 mV vs NHE (Figure 5.1). This signal grew in over time to reach a maximum size of 41 ± 4 nC and -51 ± 2 nC for the reductive and oxidative peaks at a 100 mV/s scan rate after two hours of incubation (Figure 5.1). The CV current varied linearly with the square root of the scan rate (Figure 5.2), yielding a diffusion coefficient D on the order of 7 x 10^{-6} $cm^2 \cdot s^{-1}$ upon application of the Randles-Sevcik equation. A linear dependence on the root of the scan rate is characteristic of diffusive rather than adsorbed species, which instead show a linear relationship between scan rate and current (*34*). Diffusive behavior has been observed previously for DNA repair proteins under similar conditions, and would indeed be expected for a polymerase-sliding clamp complex on a free DNA end (*14*). No differences were observed between aerobic and anaerobic electrochemistry carried out in a glove bag, indicating that the cluster is relatively stable in air and consistent with the general long-term stability of B-family DNA polymerases (*37*). The redox couple observed was attributed to the $[4Fe4S]^{3+/2+}$ based on the fact that Pol δ is HiPIP-like, being EPR-silent unless oxidized (*7*). In addition, the electrochemical signal is similar to the DNA glycosylases EndoIII and MutY, in which the identity of the couple has been established by EPR (*13*, *24*).

We could obtain quantifiable signals at lower concentrations by adding dNTPs and Mg^{2+} to enhance protein association with the DNA. To prevent degradation of the DNA substrate by

the 3′-5′ exonuclease activity of WT Pol δ, we turned to the exonuclease-deficient mutant Pol δ DV (D520V) for these experiments (*33*). At 113 ± 5 mV vs NHE, the midpoint potential of Pol δ DV is indistinguishable from WT (Figure 5.1). By adding 80 μM dATP (the incoming nucleotide), 8.0 mM $MgAc_2$, and 5.0 μM PCNA, we were able to see signals with Pol δ concentrations as low as 500 nM (Figure 5.1). Under these conditions, the maximum CV peak areas were 6.9 ± 1 nC and -7.5 ± 1 nC for the reductive and oxidative peaks at a scan rate of 100 mV/s.

The Pol δ midpoint potential as measured resides within the HiPIP regime, but it is slightly higher than the 65-95 mV vs NHE reported for DNA-bound repair proteins (*13, 28*). To determine if this was an intrinsic difference between these proteins or the result of different buffer conditions, we performed electrochemistry on the well-studied *E. coli* BER glycosylase EndoIII following exchange into Pol δ storage buffer (*28*). In standard phosphate storage buffer (20 mM sodium phosphate, pH 7.5, 100 mM NaCl, 1 mM EDTA, 10% glycerol v/v), the EndoIII midpoint potential is ~80 mV versus NHE (*28*). When we exchanged EndoIII into Pol δ storage buffer, CV and SQWV scans of 140 μM EndoIII resulted in a midpoint potential of 113 ± 3 mV versus NHE, which is indistinguishable from that of Pol δ (Figure 5.3). Notably, this result held even when EndoIII was diluted to 1.5 μM to more closely approximate the conditions used for polymerase experiments (Figure 5.3). UV-visible spectra confirmed the stability of EndoIII in Pol δ buffer (Figure 5.3a). That the EndoIII midpoint potential matches that of Pol δ confirms that there is no significant difference between the [4Fe4S] cluster between these two proteins. The potential increase in Pol δ storage buffer is thus most likely the result of higher ionic strength (350 mM NaAc in Pol δ buffer vs 150 mM NaCl in EndoIII buffer) (*38, 39*). In any

case, these results support the assertion that the [4Fe4S] cluster resides in the same narrow potential regime in a wide range of DNA-binding proteins.

Given that Pol δ ordinarily functions in complex with PCNA, we next asked what effect PCNA might have on the electrochemical properties of Pol δ. In the absence of PCNA, the midpoint potential is unaltered at 115 ± 8 mV versus NHE, but the signal was markedly smaller, reaching a maximum CV peak area of 0.4 ± 0.1 nC for the reductive peak and -0.7 ± 0.1 nC for the oxidative peak (Figure 5.4). The signal also decayed more rapidly with PCNA absent, suggesting lower polymerase stability. To more quantitatively compare the signals obtained in the presence and absence of PCNA, we measured diffusion coefficients (D) under both conditions, as well as with and without dATP, by applying the Randles-Sevcik equation to the scan rate dependence of the current (*34*). To confirm that our values were within the expected range, we also calculated D from the Stokes-Einstein equation, using a hydrodynamic radius obtained from several crystal structures. At maximum signal size, D was found to be 6.7 ± 3 x 10^{-6} $cm^2 \cdot s^{-1}$ with both PCNA and dATP present, which is within one order of magnitude of the Stokes-Einstein estimate (6.0 x 10^{-7} $cm^2 \cdot s^{-1}$). The difference between these values most likely reflects the use of simplified geometries calculated from partial crystal structures. In the absence of PCNA, D decreased by more than an order of magnitude to 1.2 ± 0.3 x 10^{-7} $cm^2 \cdot s^{-1}$, lower than either our experimental values with PCNA present or our Stokes-Einstein estimates, indicating a change in complex shape. As Pol δ has multiple contacts with PCNA, a change in shape is expected, and our result is fully consistent with earlier studies that indicates an elongate form for Pol δ alone in solution and a more compact form when bound to PCNA (*7*, *40*). To see if dNTPs can also contribute to the shape of PCNA-bound Pol δ, we prepared a surface with Pol δ and PCNA but lacking dATP and Mg^{2+}. Under these conditions, the signal is comparable to that in

the absence of PCNA, giving a D value of $2.2 \pm 0.7 \times 10^{-7}$ $cm^2 \cdot s^{-1}$ and suggesting that, even with PCNA present, Pol δ is less compact without dNTPs. Taken together, these results indicate that PCNA does not affect the potential of Pol δ but is critical for effective DNA binding. The differences in signal size and stability suggest that, at least at nanomolar concentrations, the Pol δ [4Fe4S] cluster is most strongly coupled to the electrode when both PCNA and dNTPs are present. The importance of PCNA and dNTPs to DNA binding further suggest that the signals observed were from DNA-bound protein.

Given the experimental support for the observed electrochemical signals being DNA-bound, we next aimed to determine if Pol δ can signal in a DNA-mediated fashion. To this end, we prepared multiplexed chips containing DNA modified with either an abasic site or a CA mismatch 6 nucleotides from the thiolated end (Figure 5.1). Because DNA-bound proteins are capable of charge transport both through the DNA bases and directly through the monolayer surface, we also varied monolayer morphology in these experiments (Figure 5.5) (*28*). Thiolated DNA monolayers can be self-assembled in two basic ways: overnight incubation with 100 mM $MgCl_2$ forms closely packed islands of DNA (30-50 $pmol \cdot cm^{-2}$), while standard loosely packed monolayers (15-20 $pmol \cdot cm^{-2}$) form in the absence of Mg^{2+} (Figure 5.) (*41, 42*). Loosely packed monolayers had been used exclusively to this point to avoid steric crowding with large protein complexes, but the more densely covered closely packed monolayers have been shown to be more amenable to DNA-mediated signaling in experiments with EndoIII (*28*). To test each of these conditions, chips were prepared with one of the two monolayer forms, with the device divided evenly between well-matched and either abasic or CA mismatch DNA (Figure 5). All experiments were performed with 500 nM Pol δ DV in the presence of PCNA, dATP, and $MgAc_2$.

Consistent with previous studies on EndoIII (*28*), Pol δ redox potentials were identical on both film morphologies, supporting the assertion that all observed signals are from DNA-bound proteins (Figure 5). On closely packed DNA films, signal size was highly variable, but 46 ± 33% signal attenuation as determined by SQWV occurred on abasic DNA (Figure 5.5). No mismatch discrimination was observed, and even the abasic site discrimination decreased over time as more protein diffused to the surface. In general, the signals on closely packed monolayers are consistent with significant steric hindrance causing protein-DNA complexes to lie flat on the surface (Figure 5.5b). In contrast, signals on loosely packed monolayers were of very consistent size and showed significant charge attenuation with both abasic and CA-mismatch DNA, reaching maxima of 44 ± 16% on abasic DNA and 46 ± 29% on CA-mismatch DNA after 2 hours of incubation as measured by SQWV (Figure 5.5). Abasic site and mismatch discrimination remained stable over several hours, suggesting less steric hindrance not on loosely packed DNA. Together, these results confirm that Pol δ is capable of DNA-mediated signaling and emphasize the importance of substrate accessibility when assessing CT by large protein complexes.

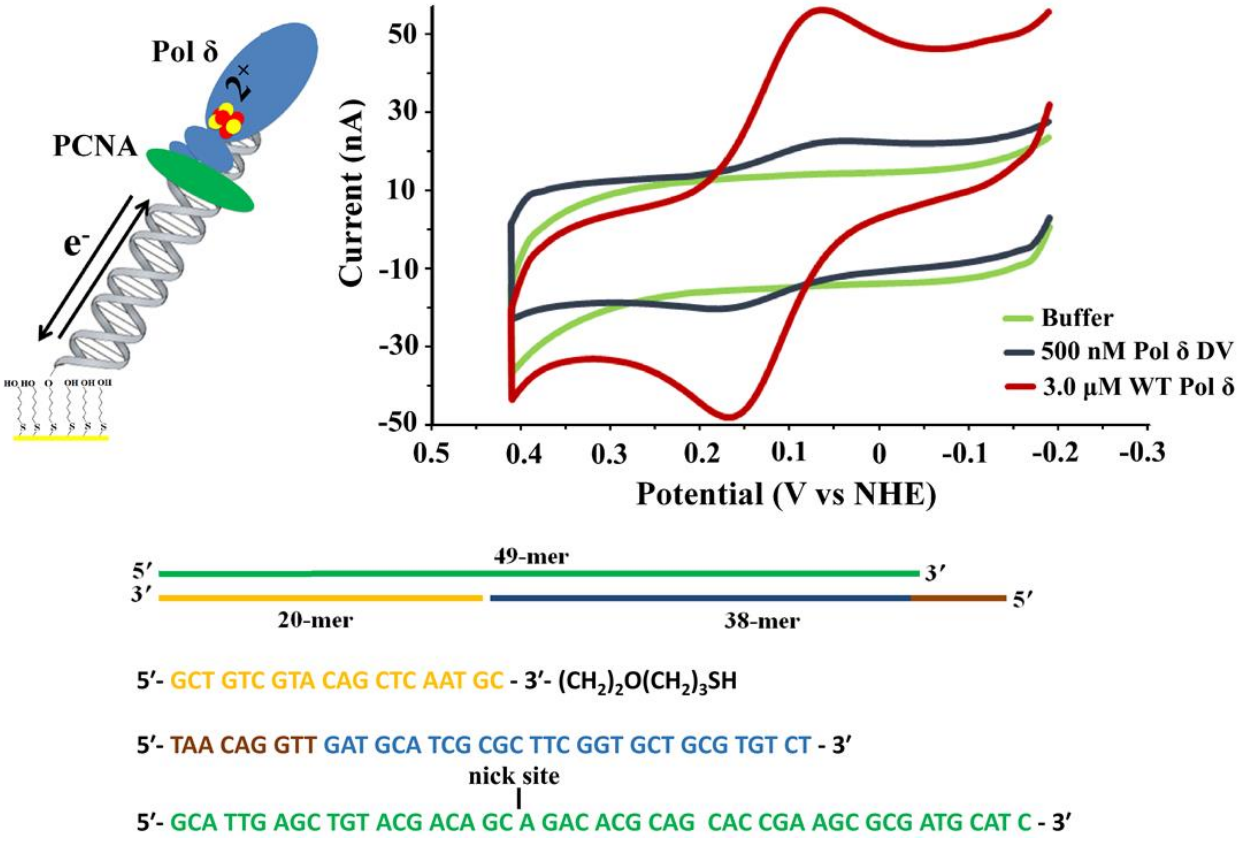

Figure 5.1 Cyclic voltammetry with WT and exonuclease-deficient Pol δ. (**Top**) The addition of 3.0 μM WT Pol δ and 10 μM PCNA to a DNA-modified gold electrode resulted in a reversible CV signal with a midpoint potential centered at 113 ± 4.7 mV versus NHE (red trace). By using the exonuclease deficient mutant Pol δ DV, which cannot degrade DNA in the presence of catalytic magnesium, signals could be obtained at concentrations as low as 500 nM when $MgAc_2$, 5 μM PCNA and excess dATP were included (blue trace). As expected, WT Pol δ and Pol δ DV have indistinguishable midpoint potentials at 116 ± 3 and 113 ± 3 mV versus NHE, respectively. (**Bottom**) DNA substrate design for electrochemical experiments. The substrate consists of 3 parts, a 20-mer thiol, a 38-mer and a 49-mer complement. Notably, the nick in the phosphate backbone is not expected to interfere with CT. Electrochemistry was performed in storage buffer (30 mM HEPES, pH 7.4, 350 mM NaAc, 1 mM DTT, 0.1 mM EDTA, 10% glycerol v/v, 0.01% decaethylene glycol monododecyl ether v/v), and the abasic site/mismatch discrimination experiments also included 5.0 μM PCNA, 80 μM dATP, and 8.0 mM $MgAc_2$. All CV scans were taken at a scan rate of 100 mV/s.

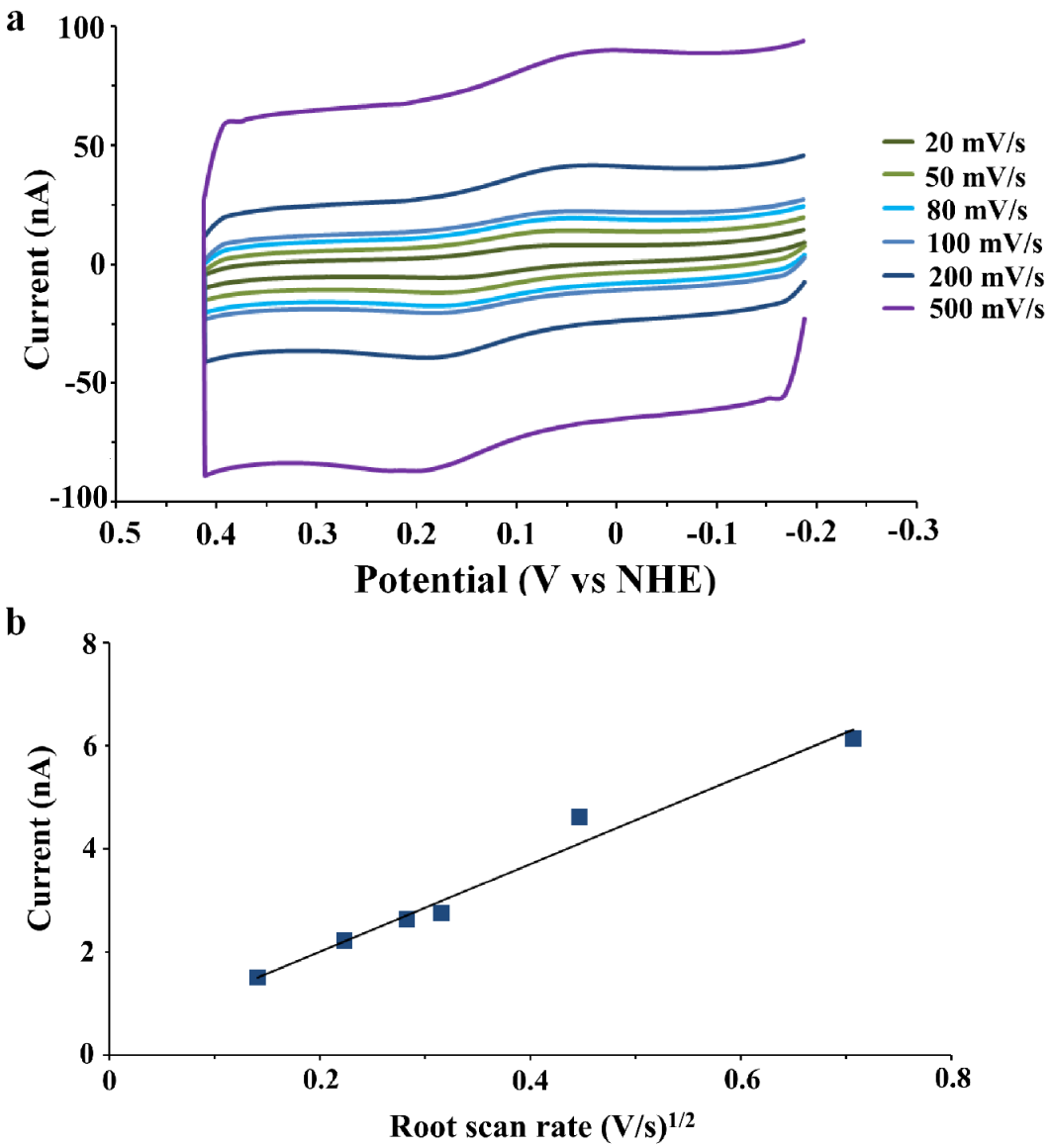

Figure 5.2 Scan rate dependence of the CV current in 500 nM Pol δ DV incubated with 5.0 μM PCNA, 80 μM dATP, and 8.0 mM $MgAc_2$. (**a**) The maximum peak current increases with increasing scan rate, coupled with an increase in peak splitting. (**b**) The current exhibits a linear dependence on the square root of the scan rate, characteristic of a diffusive rather than adsorbed species. The scan rates included are 20, 50, 80, 100, 200, and 500 mV/s. The line was fit to data averaged from 8 separate experiments, and the fit is $I = 7.7559\nu^{1/2} + 0.5725$ with an R^2 value of 0.9828.

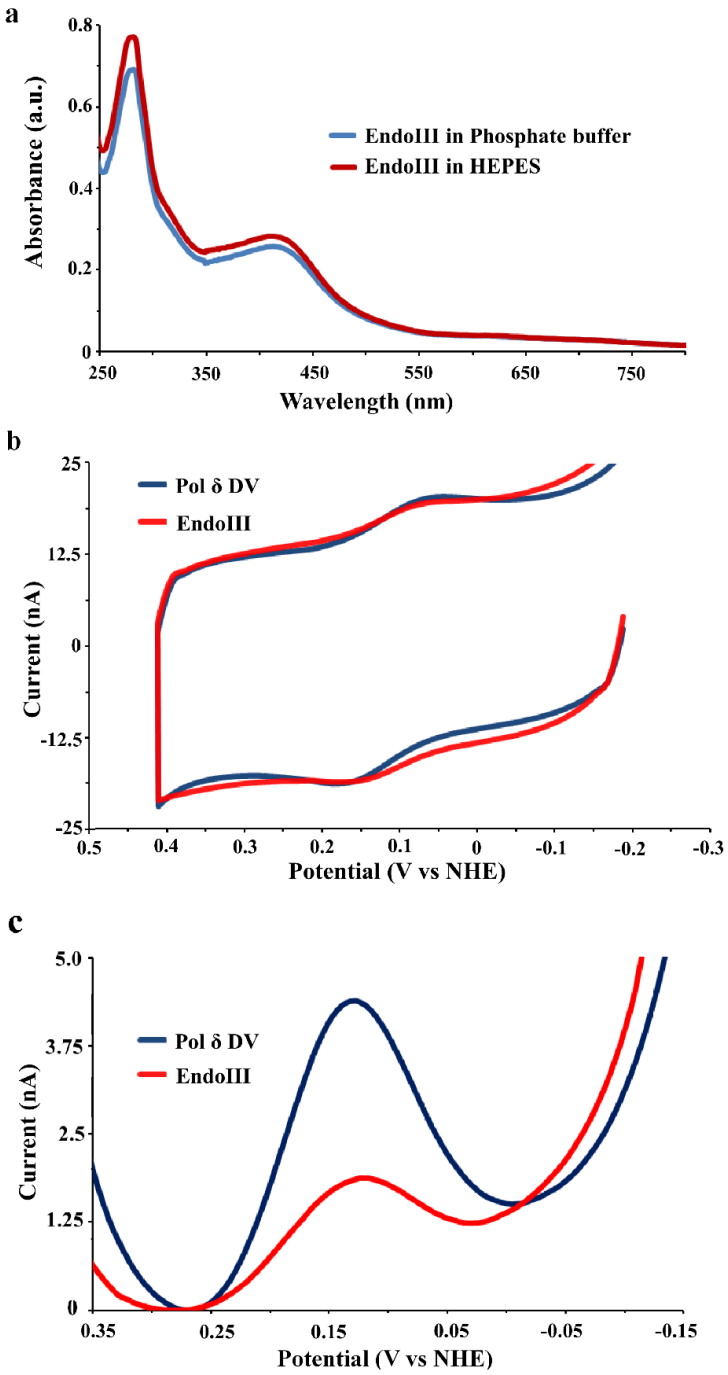

Figure 5.3 Pol δ and EndoIII electrochemistry compared. 1.5 μM EndoIII (stored in 20 mM sodium phosphate, pH 7.5, 150 mM NaCl, 1 mM EDTA) was exchanged into Pol δ storage buffer (30 mM HEPES, pH 7.4, 350 mM NaAc, 1 mM DTT, 0.1 mM EDTA, 10% v/v glycerol, 0.01% decaethylene glycol monododecyl ether w/v) and added to a multiplexed chip containing unmodified Pol δ DNA (49:58-mer substrate). (**a**)UV-visible spectra taken before and after buffer exchange confirm the stability of EndoIII in a HEPES-based buffer. (**b**) The midpoint potential as measured by CV is 113 ± 3 mV, virtually indistinguishable from Pol δ DV at 113 ± 5 mV versus NHE.

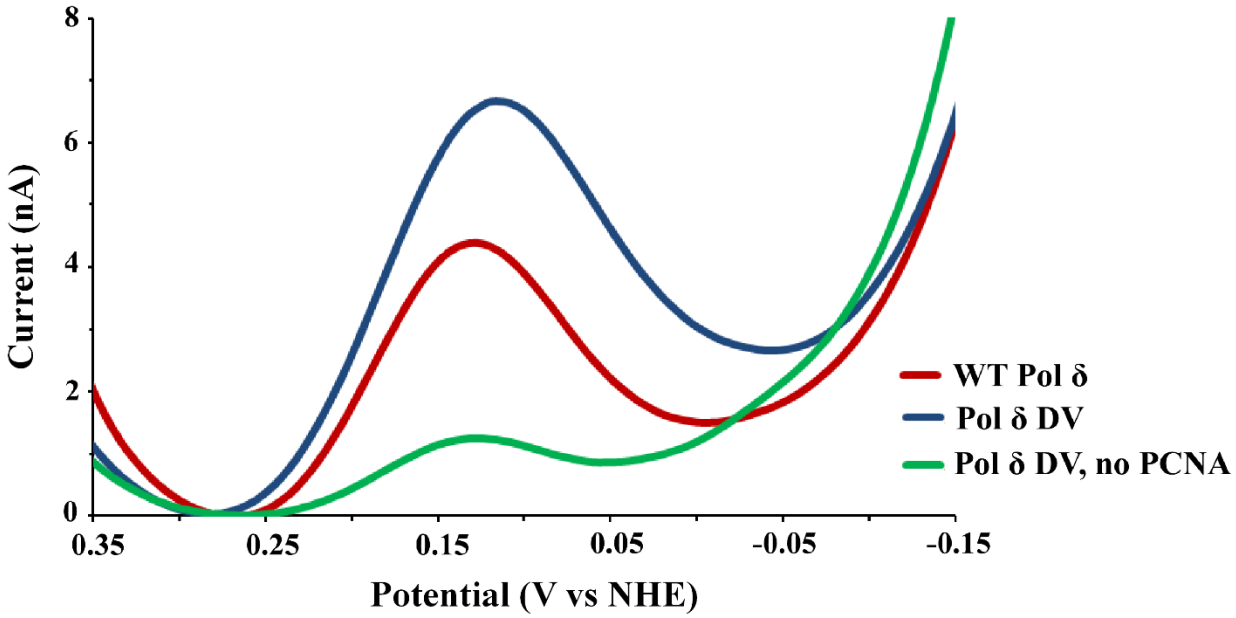

Figure 5.4 SQWV of 500 nM WT Pol δ and exonuclease-deficient Pol δ DV with and without 5.0 μM PCNA. WT and exo$^-$ Pol δ DV share the same potential, and both generate a substantial signal on a DNA-modified gold electrode; the smaller size of the WT signal may be due in part to DNA degradation by exonuclease activity. PCNA itself does not affect the potential, but its absence results in significantly decreased signal size and lower stability over time. SQWVs were taken at 15 Hz frequency and 25 mV amplitude, and electrochemistry was carried out in storage buffer (20 mM HEPES, pH 7.4, 350 mM NaAc, 1 mM DTT, 0.1 mM EDTA, 10% glycerol v/v, 0.01% decaethylene glycol monododecyl ether v/v) with 8.0 mM $MgAc_2$ and 80 μM dATP.

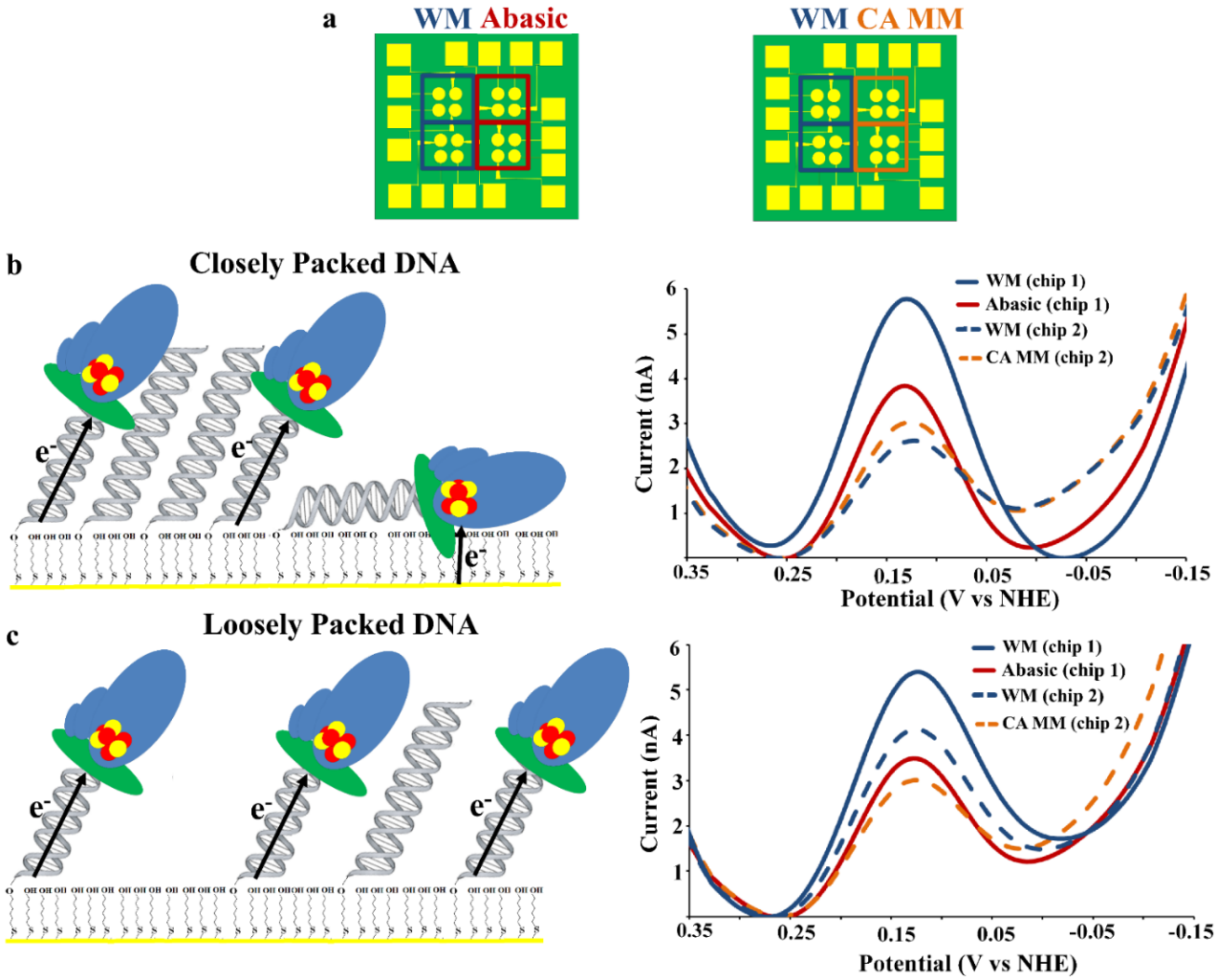

Figure 5.5 Pol δ electrochemistry on different DNA monolayer morphologies. (**a**) To find an optimal DNA monolayer morphology for Pol δ signaling, we prepared multiplexed chips containing either closely packed (assembled with 100 mM $MgCl_2$) or loosely packed (no $MgCl_2$) DNA films. Two chips were prepared for both morphologies, with one half of each chip consisting of well-matched (WM) DNA (dark blue) and the other containing DNA with either an abasic site (red) or a CA mismatch (orange) 6 nucleotides from the monolayer surface. (**b**) On closely packed films, Pol δ SQWV signals were highly variable and showed 46 ± 33% attenuation on abasic DNA (solid SQWV traces) but no significant mismatch discrimination (dashed SQWV traces). (**c**) In contrast, SQWV signals on loosely packed films were much more consistent between electrodes, with a 44 ± 16% signal loss on abasic DNA (solid traces) and 46 ± 29% signal loss with CA mismatch DNA (dashed traces). To minimize the effects of variability between devices, all direct comparisons were made on a single chip; scans that were directly compared are denoted by either solid or dashed lines in the SQWV signals shown. The SQWV traces shown are an average of 6 individual electrodes on a single device, with scans taken at 15 Hz frequency and 25 mV amplitude.

Activity Assays with Oxidized and Reduced Pol δ

Having seen that DNA binding can activate Pol δ for redox activity, we next asked if the cluster oxidation state might affect polymerase activity. As purified, Pol δ exists largely in the $[4Fe4S]^{2+}$ state (*7*), so any assessment of activity differences would require extensive oxidation to generate sufficient amounts of the $[4Fe4S]^{3+}$ cluster for comparison. For this task, we used bulk electrolysis on DNA-modified electrodes, applying an oxidizing potential of 0.412 V versus NHE for 15-20 minutes under an inert atmosphere (95% N_2/5% H_2) to prevent cluster degradation (Figure 5.6a).

High bulk electrolysis yields generally require an electrode with substantial surface area, so we switched from multiplex chips to single gold rod electrodes for these experiments. Multiplexed chips have many advantages for electrochemical characterization, but only a single electrode can be addressed at a time and each sample in a quadrant is distributed across 4 separate electrodes. To confirm the effectiveness of this system, a sample of concentrated (150 μL of 2.74 μM) Pol δ was oxidized on a DNA-modified electrode in a custom-made glass cell for several hours (Figure 5.6b). UV-visible spectra were taken before and after electrolysis, after which the sample was then frozen for EPR in parallel with untreated protein (Figure 5.6c, d). The [4Fe4S] cluster oxidation generally results in a broad increase in UV-visible absorbance from 300-450 nm with a less distinct peak at 410 nm in both the $[4Fe4S]^{3+}$ and $[3Fe4S]^{+}$ species (*43*–*45*). After bulk electrolysis, increased absorbance from 300-400 nm, consistent with cluster oxidation, was indeed observed. No significant increase in absorbance at 800 nm occurred after oxidation, and the 280 nm peak associated with aromatic and thiolated amino acid residues remained distinct. From our own observations, protein aggregation tends to generate a U-shaped curve with high absorbance at 800 nm and a shallow, poorly defined peak at 280 nm, and the

lack of these features in our spectra indicate that oxidized Pol δ did not aggregate (Figure 5.6c). EPR signals are small as a result of the low sample concentration, but clear signals at g = 2.08 and g = 2.02 are present in the oxidized sample (Figure 5.6d). These signals are consistent with a combination of $[4Fe4S]^{3+}$ and $[3Fe4S]^{+}$ cluster oxidation products (*24*, *44-45*). A smaller signal at g = 2.02 was also present in the native sample, consistent with earlier reports of residual $[3Fe4S]^{+}$ cluster in untreated Pol δ (*7*). That some $[3Fe4S]^{+}$ cluster would occur upon oxidation is not surprising, and similar results have been obtained for EndoIII and MutY (*13*, *24*). In earlier studies, loss of iron was attributed in part to damage incurred upon freezing, which may have also happened here. Furthermore, oxidized Pol δ was stored away from protective DNA long enough to take a UV-visible spectrum prior to freezing. In any case, some $[4Fe4S]^{3+}$ cluster was still observed, and the $[3Fe4S]^{+}$ cluster that did occur would have formed as a degradation product of the $[4Fe4S]^{3+}$ cluster (*13*).

Because activity assays require only low nanomolar polymerase concentrations, bulk electrolysis for these experiments was carried out with 190 nm Pol δ DV to minimize sample waste. Oxidation yields under these conditions were higher, typically around 75 – 90% as determined from the total charge passed. After electrolysis, untreated or oxidized Pol δ DV was added directly to pre-made reaction mixes to a final concentration of 2 nM (Figure 5.7a). When run out on an alkaline agarose gel, it is apparent that at early time points less DNA synthesis was carried out by oxidized Pol δ (Figure 5.7, 8). DNA synthesis can be more quantitatively compared for the oxidized versus untreated sample by dividing the amount of frontier products (highest molecular weight major products) in the oxidized sample by the amount present in untreated samples. Using this analysis, oxidized Pol δ at 60-80% yield forms only 30-50% as many large (~ 5 kb) DNA products as untreated Pol δ after 30 seconds (Figure 5.7c).

Significantly, higher oxidation yields lead to lower activity levels. In any case, this difference gradually decreases over the course of 10 minutes. Regardless of oxidation state, no DNA synthesis occurs in samples lacking PCNA, confirming that all observed DNA synthesis is processive (Figure 5.8c).

Reduction of the oxidized Pol δ stock by electrolysis at -0.188 V versus NHE effectively restores DNA synthesis, reaching 90% of untreated levels at early time points (Figure 5.7, 8). Critically, this result both confirms the reversibility of oxidative slowing and provides support for the $[4Fe4S]^{3+}$ cluster as the major oxidation product. As mentioned earlier, the reversible electrochemical signals are consistent with $[4Fe4S]^{3+/2+}$ cycling, but EPR spectroscopy with oxidized Pol δ showed evidence of both $[4Fe4S]^{3+}$ and $[3Fe4S]^{+}$ products in the sample, leading to some ambiguity. However, the nearly complete restoration of native activity levels upon re-reduction would not be expected if most of the cluster had degraded to the $[3Fe4S]^{+}$ state, supporting the $[4Fe4S]^{3+}$ cluster as the major oxidation product. These combined results thus indicate that the $[3Fe4S]^{+}$ cluster seen by EPR likely forms after the $[4Fe4S]^{3+}$ major product degrades over time in the absence of DNA; we have observed this previously with sample freezing for *E. coli* EndoIII and MutY following chemical oxidation (*13, 24*).

To gain further insight into the effect of oxidation, reaction rates were estimated by comparing frontier velocities. Velocities were calculated by dividing the amount of the largest quantifiable band of DNA by time and the number of polymerase molecules present (*46*). This method yields maximum rates of 118 ± 63 (SD, n = 7) nt/s per enzyme for untreated Pol δ and 21 ± 27 (SD, n = 5) nt/s for oxidized Pol δ at 2 minutes. The rates obtained for untreated Pol δ are consistent with previously published *in vitro* results (*35*), while the oxidized form is significantly slower. This calculation represents just an upper estimate, as typical bulk electrolysis fails to

oxidize around 20-30% of the enzyme; thus, some of the DNA synthesis observed in oxidized samples can be attributed to the non-oxidized population. Indeed, the comparable amounts of DNA synthesis observed after 5-10 minutes could have resulted from either slow oxidized polymerase catching up or redistribution by of residual native Pol δ in the oxidized sample. Overall, it is clear from these experiments that oxidation leads to a decrease in replication rate, but resolution on alkaline agarose gels is insufficient to distinguish between complete stalling or dramatic slowing of DNA synthesis.

To distinguish between stalling and slowing of DNA synthesis by oxidized Pol δ, reactions were analyzed on 5% polyacrylamide gels to obtain increased resolution in the 30-1000 nucleotides range. In addition, DNA synthesis was limited to that of a single processive cycle by the PCNA-Pol δ complex by adding heparin, which traps dissociated Pol δ (*35*). Without the heparin trap, products up to 7 kb were observed, due to multiple processive cycles of synthesis (Figure 5.7, 8). In order to visualize products at all sizes, reactions containing heparin were divided in two, with half loaded onto a polyacrylamide gel and half onto an alkaline agarose gel. With heparin present, alkaline agarose gels demonstrate a severe limitation to DNA synthesis, with no products larger than ~1 kb observed on alkaline agarose gels (data not shown). When these products are resolved on polyacrylamide gels, a greater proportion of both very small (~primer length) and very large (~1 kb) products are formed by untreated Pol δ, while the oxidized form generates more intermediate products between 30 and 1000 nucleotides (Figure 5.9).

These results illustrate several important points about the effects of oxidation on Pol δ DNA synthesis. First, they verify that the oxidized form remains active and does not completely stall. Second, the relatively greater amounts of very small products and unextended primers in

reactions with native sample indicate greater susceptibility to dissociation from DNA and trapping by heparin, while the native form that does associate produces longer products. In contrast, oxidized Pol δ leaves fewer primers unextended or fully extended, instead making more intermediate products between 150 bp and 1 kb. The greater proportion of extended primers is consistent with tighter DNA binding after cluster oxidation, as has been observed with both primase and DNA repair proteins (*16, 27*). However, the slower procession indicates that tighter binding impedes rapid procession, acting as a brake on PCNA-mediated DNA synthesis. These experiments suggest that the similar activity levels observed on alkaline agarose gels at time points beyond 5 minutes could be explained by either the oxidized form gradually catching up or by redistribution of the residual native enzyme in the sample. Regardless of the precise details, the overall impact of polymerase stalling, with a 6-fold decrease in rate, would be significant on the timescale of S-phase; unperturbed yeast S-phase lasts ~30 minutes, while using oxidized Pol δ moving at 20 nt/s to replicate the lagging strand of the yeast genome would itself require 27 minutes (*47-49*).

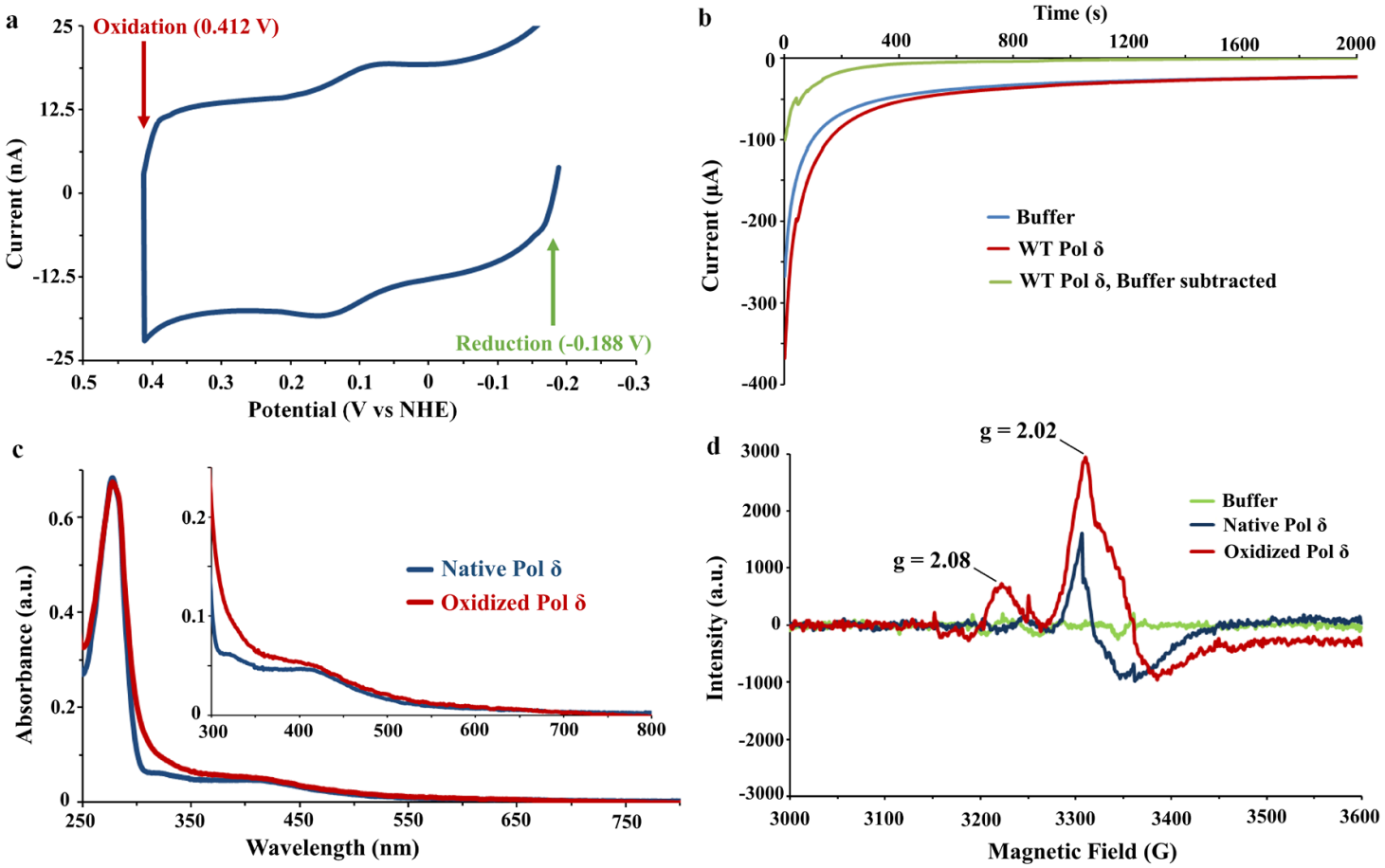

Figure 5.6. Characterization of electrochemically oxidized Pol δ. (**a**) Bulk electrolysis potentials were ~200 mV beyond the major oxidative and reductive peaks at 0.412 V (oxidation) and -0.188 V (reduction) versus NHE. (**b**) Yields were calculated by subtracting a background electrolysis (blue) from one containing protein (red) and taking the area under the resultant curve (green). Electrolysis of 150 µL of 2.74 µM Pol δ at 0.412 V gave ~35% oxidation yield. (**c**) UV-visible spectra reveal an increased absorbance from 300-400 nm consistent with cluster oxidation with no evidence of protein aggregation. (**d**) CW X-band EPR spectra at 10 K reveal the presence of both $[4Fe4S]^{3+}$ (g = 2.08) and $[3Fe4S]^{+}$ (g = 2.02) species in the oxidized sample, with a residual amount of $[3Fe4S]^{+}$ cluster present in the native sample. These results are consistent with the formation of $[4Fe4S]^{3+}$ cluster after anaerobic bulk electrolysis, with some degrading to form $[3Fe4S]^{+}$ cluster in the absence of DNA. As slight sample loss did occur following oxidation, the UV-visible spectrum of oxidized Pol δ has been normalized to native absorbance at 280 nm to afford a more direct comparison. EPR spectra were taken at 12.85 mW microwave power, 2 G modulation amplitude, and a receiver gain of 5.02 $x10^3$.

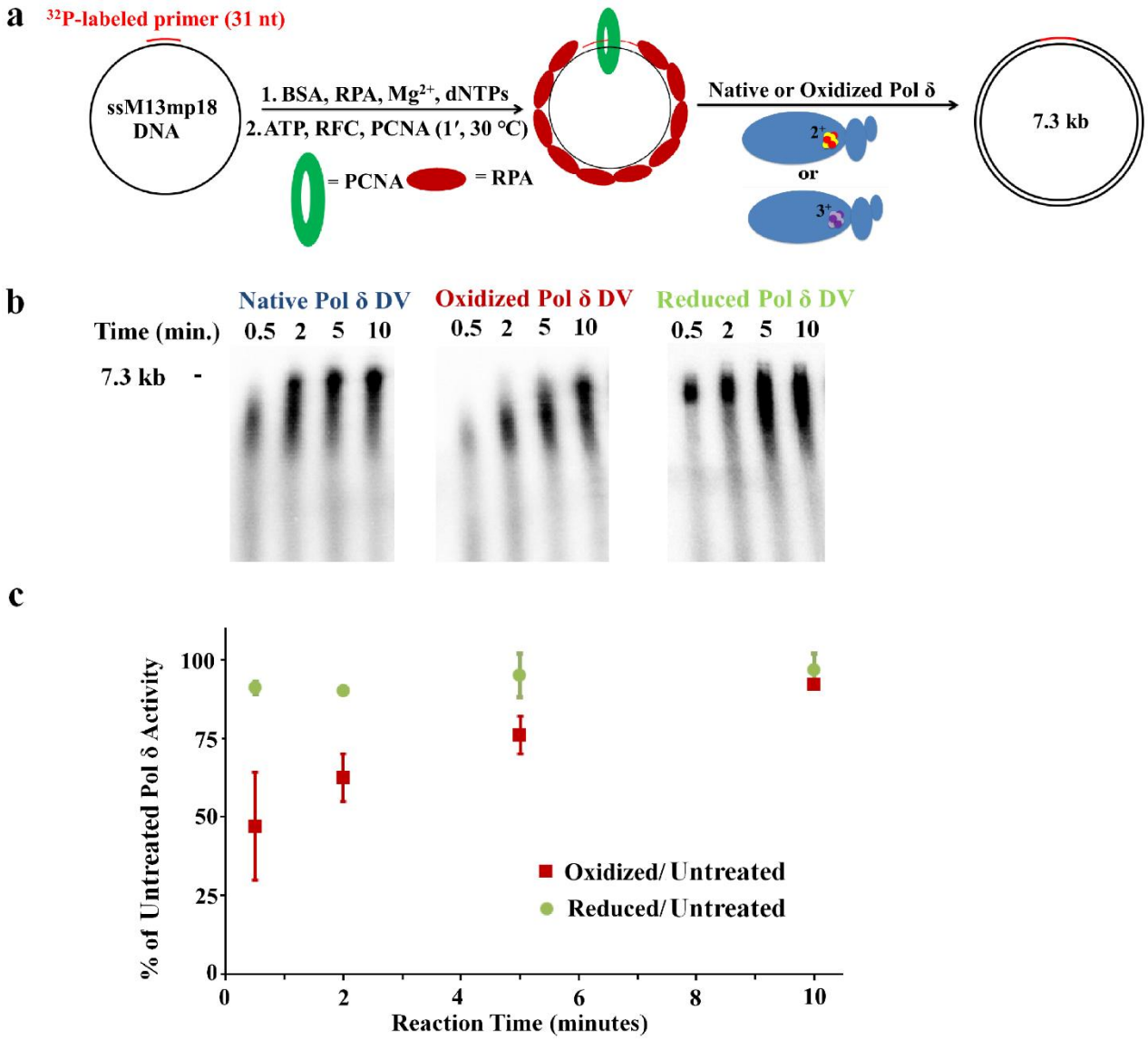

Figure 5.7 Activity assays with native and electrochemically oxidized Pol δ DV. (**a**) 190 nM Pol δ DV was oxidized or reduced by bulk electrolysis at potentials of 0.412 V and -0.188 V and subsequently diluted to 2 nM final concentration into reaction mixes containing radiolabeled M13mp18 DNA. (**b, c**) As seen on representative 1% alkaline agarose gels, oxidation lowers activity levels at early time points, while reduction restores activity to native levels. The degree of this effect can be quantified by dividing the amount of DNA synthesis in reactions with oxidized or reduced Pol δ by that from reactions with untreated enzyme. The oxidation yield for the gel shown in **b** is ~80%. Error bars are standard deviation of the mean ($n \geq 3$).

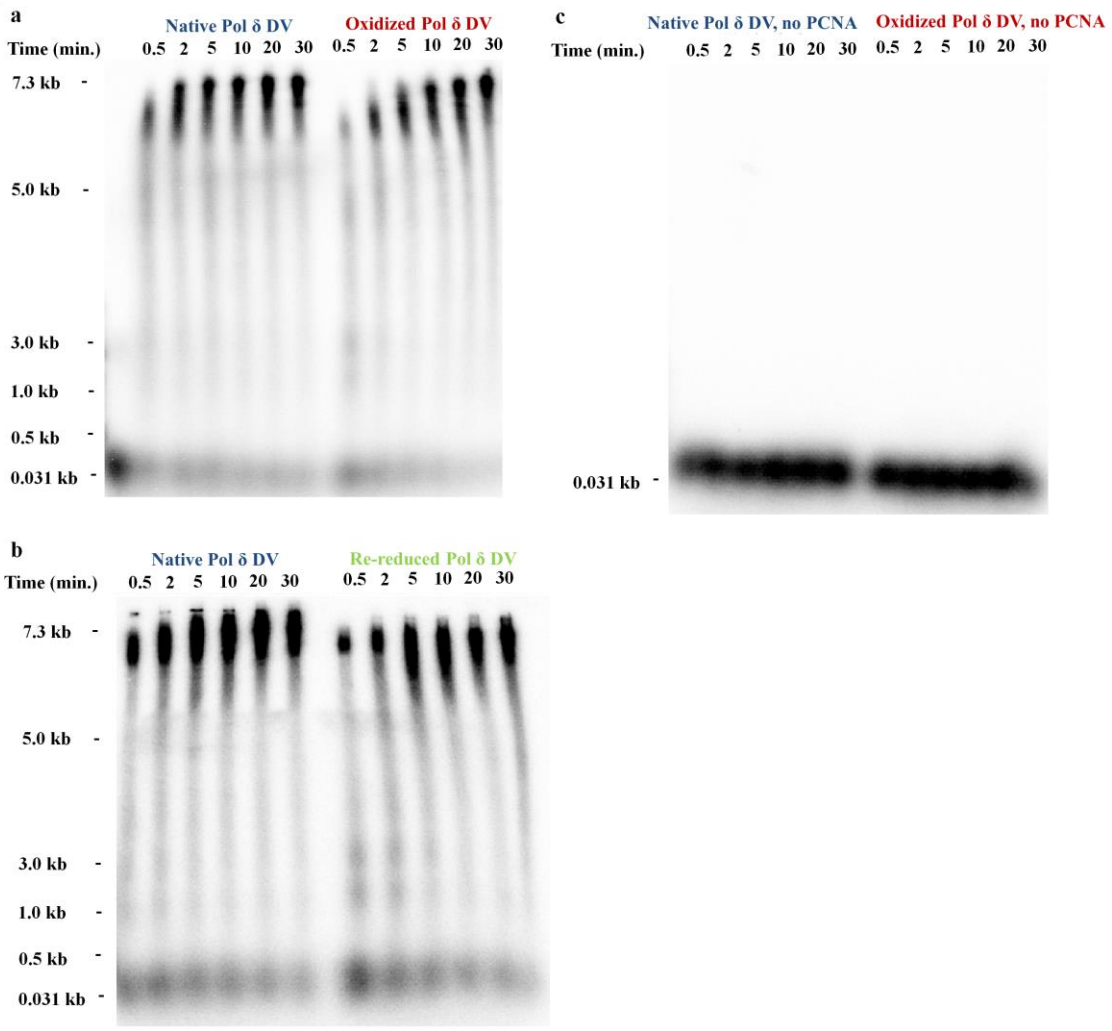

Figure 5.8 Complete alkaline agarose gels from Figure 5.7 and control lacking PCNA. The gels include untreated and oxidized Pol δ DV with 5.0 nM PCNA (**a**), untreated and re-reduced Pol δ DV (**b**), and untreated and oxidized Pol δ DV in the absence of PCNA (**c**). No DNA synthesis occurs in the absence of PCNA, confirming that the observed activity in native and oxidized samples is processive.

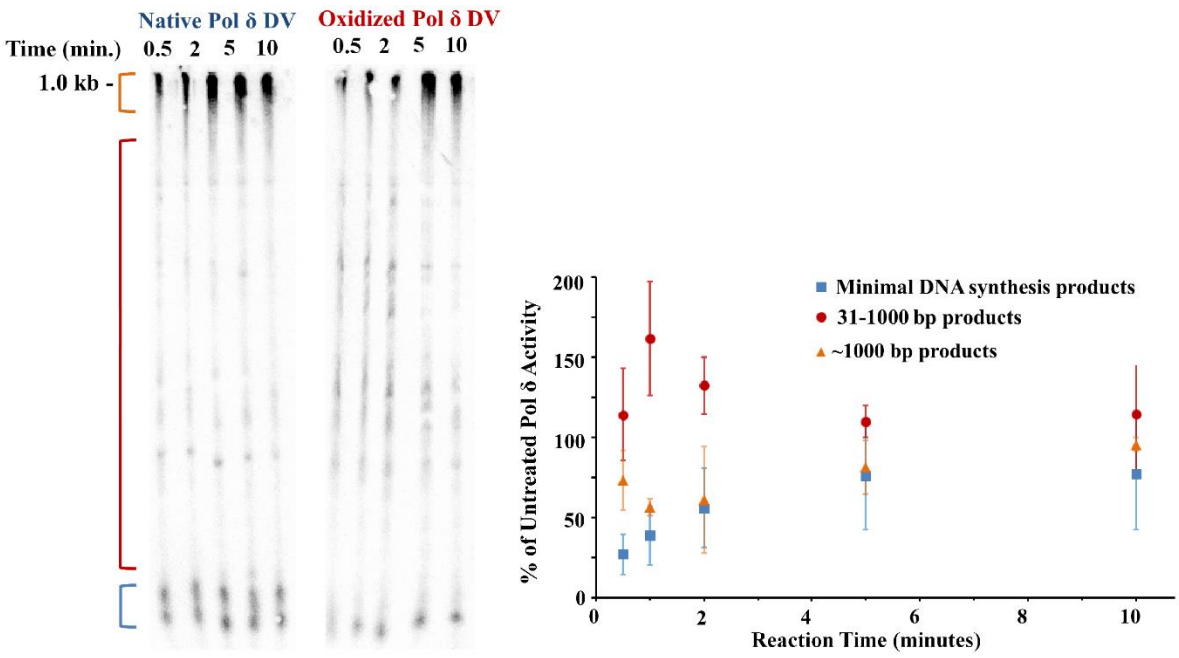

Figure 5.9 Establishment of activity by oxidized Pol δ. To see if oxidized Pol δ remained active or stalled completely, 0.01% heparin was included in reactions to challenge synthesis and products were analyzed on a 5% denaturing polyacrylamide gel to resolve DNA between 30 and 1000 bp (left). Pol δ remains active after oxidation, primarily forming intermediate-sized products (red range on gel). Native Pol δ is more sensitive to heparin, with more DNA close to primer length (blue range), but when it does associate with DNA, most products are around the maximum size (orange range). These results are consistent with tighter binding and slower processive DNA synthesis by the oxidized form. Gels were quantified using ImageQuant software; as synthesis appears as smears at this resolution, the total amount of background-subtracted radioactivity in each major range shown was compared between untreated and oxidized Pol δ. Error bars are standard deviation of the mean (n = 3).

Chemical Oxidation of Pol δ with Anthraquinone

Electrochemical oxidation provides clear advantages in estimating yields and re-reducing the oxidized sample, but the use of chemical oxidants is much more common. Thus, we were interested to see if chemical oxidation could yield an equivalent result. To this end, we used an anthraquinone (AQ)-derived photooxidant covalently tethered to the 5′ end of the DNA primer (*36, 50*). AQ has the advantage of oxidizing samples in a DNA-mediated fashion instead of the less effective, direct oxidation of the protein by oxidants in solution (*7, 50*). Irradiation at 350 nm of AQ generates an excited triplet state capable of oxidizing DNA bases, and AQ has been studied extensively in the context of DNA CT (*50-52*). The DNA base of lowest potential, guanine, has a redox potential of 1.29 V, which is considerably higher than that of the Pol δ [4Fe4S] cluster at 113 mV (*53*). The presence of AQ on the primer, however, prevents 5′ ^{32}P end-labeling, so [α-^{32}P] dATP added to reactions was used as an alternative label (Figure 5.10a). Since [α-^{32}P] dATP is not necessarily incorporated in a 1:1 ratio with DNA-primed ends, activity levels were compared by total scintillation counts rather than by directly quantifying gel bands.

Following irradiation, samples with AQ showed lower overall DNA synthesis relative to identical samples kept in the dark (Figure 5.10b, c). As with electrochemistry, the maximum differentials occur at earlier time points. After 30 and 60 seconds, irradiated Pol δ showed 40-60% of dark control DNA synthesis. In contrast, reaction mixes irradiated in the presence of unmodified DNA are not significantly different from dark controls at early time points, and remain equal or greater throughout the time course (Figure 5.10c, 11). Similarly, no significant differences are observed between reactions with irradiated or untreated *E. coli* Klenow fragment exo$^-$ on AQ-modified DNA (Figure 5.11), indicating that the attenuation observed in Pol δ DNA synthesis can be attributed to [4Fe4S] cluster oxidation. Assuming the activity differential at

early time points approximated the percentage of oxidized sample, as was the case electrochemically, photooxidation yields ranged from 40-50%. Overall, the pattern of attenuated activity after photooxidation is consistent with the results from electrochemical experiments (Figure 5.10c), independently confirming the slowing of Pol δ upon cluster oxidation.

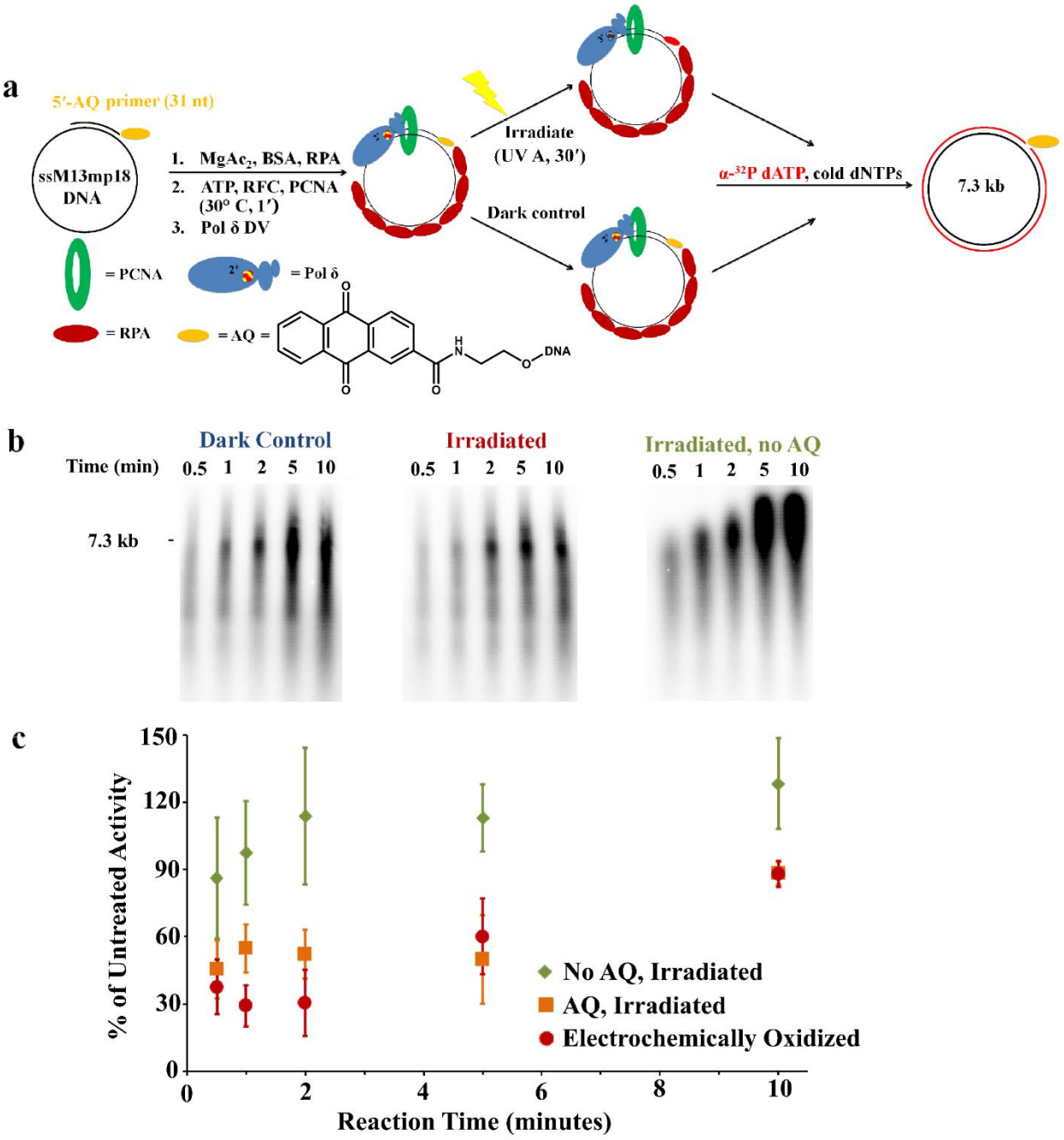

Figure 5.10 Pol δ activity assays with an AQ photooxidant. (**a**) Pol δ DV was added to a reaction mix lacking dNTPs and either irradiated under a solar simulator (UVA) or left in the dark, after which dNTPs (including [α-^{32}P] dATP) were added to start the reaction. (**b, c**) 1% alkaline agarose gels show less DNA synthesis by irradiated Pol δ at early time points, matching the pattern of electrochemical oxidation. Irradiation in the absence of AQ resulted in no significant effects, indicating that AQ was oxidizing the cluster. This pattern is apparent in relative radioactivity counts (or gel quantification for electrochemical oxidation), which further emphasize the similarity between oxidation methods. Error bars are standard deviation of the mean ($n \geq 3$).

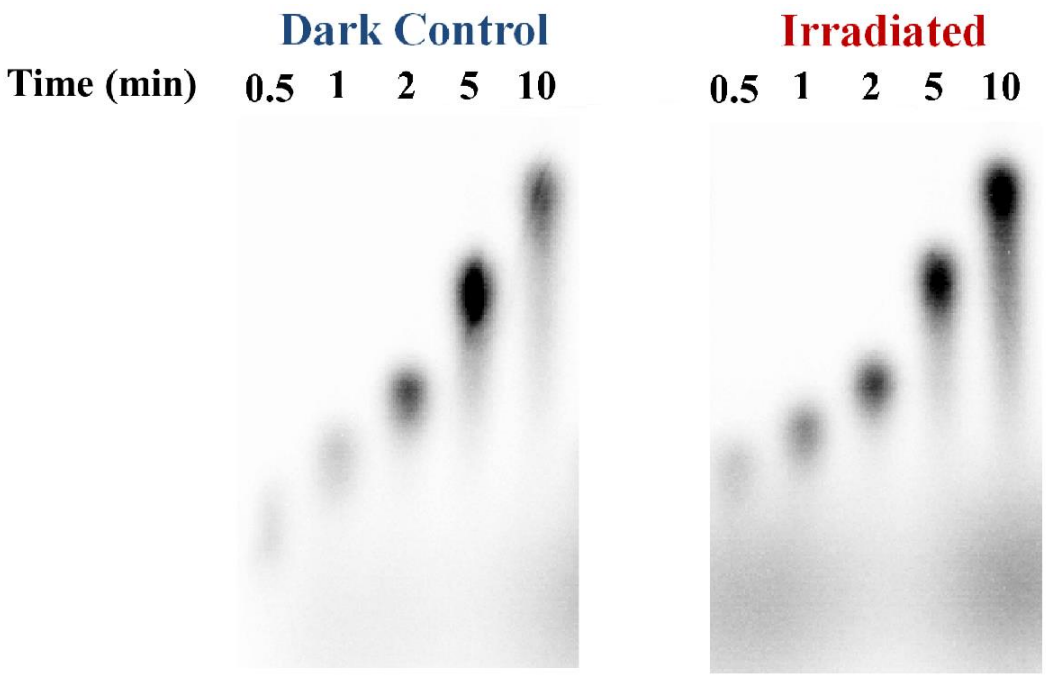

Figure 5.11 AQ assay controls with 140 nM *E. coli* Klenow fragment exo$^-$. UVA irradiation in the presence of AQ-primed DNA had no significant effect on DNA synthesis by Klenow fragment. The lack of difference confirms that irradiation in the presence of AQ does not adversely affect polymerase enzymes, and further supports the assignment of attenuated activity in Pol δ under the same conditions to [4Fe4S] cluster oxidation.

Discussion

In this work, we have demonstrated that the [4Fe4S] cluster of DNA polymerase δ can serve an important functional role as a redox-active cofactor that regulates enzymatic activity. On DNA-modified gold electrodes, Pol δ shows a reversible signal with a midpoint potential of 113 ± 5 mV versus NHE. Notably, this potential is comparable to that of the previously characterized [4Fe4S] protein EndoIII under the same buffer conditions. Charge attenuation in the presence of either an abasic site or a CA mismatch confirms that the redox signal is DNA-mediated. Activity assays carried out with electrochemically oxidized Pol δ demonstrate that oxidation results in significant slowing of processive DNA synthesis; the same result occurs following irradiation in the presence of an anthraquinone photooxidant. An assessment of both large and small DNA products indicates that the oxidized form remains active, but it is less processive. Given the retention of activity with decreased processivity, these results are consistent with an increase in DNA binding affinity upon oxidation, which would impede rapid sliding of PCNA-bound Pol δ. A significant increase in DNA binding is evident also with EndoIII upon oxidation (*27*). Critically, reduction by bulk electrolysis largely restores activity to native levels, confirming that cluster oxidation acts as a reversible switch. The reversibility of oxidation also lends further support to our electrochemical and spectroscopic evidence for the $[4Fe4S]^{3+}$ cluster as the biologically relevant oxidation product rather than degraded $[3Fe4S]^{+}$ cluster. Taken as a whole, these results suggest that reversible oxidation of the [4Fe4S] cluster in Pol δ could provide a rapid and reversible way to respond to replication stress.

Replication stress is a general term for fork slowing or stalling due to factors such as dNTP depletion, UV irradiation, and oxidative stress (*54*). Both replicative helicases and polymerases are known to be stabilized at stalled forks independently of checkpoint kinase

activity, although the mechanism of stabilization and its relationship to global checkpoint regulation remains incompletely understood (*55*). Pol δ slowing through cluster oxidation would be a straightforward way to stall replication on the lagging strand, and this form of slowing could also complement more standard regulatory mechanisms. In general, Pol δ slowing would lead to accumulation of single-stranded DNA and RPA on the lagging strand, activating checkpoint kinases that could then stall the helicase by phosphorylation of key subunits (*56, 57*). Among other types of stress, oxidative stress and ionizing radiation carry a heightened risk of double strand break formation (*58*). Furthermore, reactive oxygen species generate lesions such as 8-oxoguanine (OxoG), which is highly mutagenic due to the propensity of replicative polymerases to generate OxoG:A mispairs (*59*). Oxidation of the [4Fe4S] cluster from the 2+ to 3+ form could either occur directly, by reactive oxygen species, or, more likely, by charge transport (CT) communication through double stranded DNA with other oxidized species. Previously, we have seen that guanine radicals, the precursors to OxoG, can carry out DNA CT to oxidize the [4Fe4S] cluster of DNA-bound EndoIII (*24*). An additional benefit of polymerase stalling by DNA-mediated oxidation would be the prevention of excessive DNA synthesis under high risk circumstances. In addition to preventing damage, redox signaling to and from Pol δ could play a role in fork reversal and recombination events associated with replication stress (*54, 60*).

A general model for redox regulation of Pol δ is shown in Figure 5.12. In this model, processive lagging strand replication proceeds until replications stress occurs and the Pol δ $[4Fe4S]^{2+}$ cluster is oxidized either directly or by an electron acceptor, possibly an oxidized [4Fe4S] protein or a guanine radical formed during oxidative stress. We have found, in the case of EndoIII, that cluster oxidation promotes a substantial increase in binding affinity (*27*). Here, given the already tight binding to DNA of Pol δ with PCNA, a still tighter binding causes Pol δ

to slow its progression. The slowing of lagging strand synthesis would lead to RPA accumulation and an activation of checkpoint signaling, ultimately resulting in repair or replication fork collapse. Once the conditions of stress resolve, lagging strand synthesis can be restored by reduction of the Pol δ $[4Fe4S]^{3+}$ cluster, likely by another [4Fe4S] protein involved in DNA processing. Importantly, only Pol δ bound to the DNA in a complex with PCNA is readily oxidized, leaving the bulk of unbound Pol δ in the reduced 2+ form. Furthermore, this signaling can occur rapidly and at distance through DNA-mediated CT.

It is interesting to consider the many possible partners for DNA CT with Pol δ in the context of this model. First, Pol δ could be directly oxidized by species formed during oxidative stress, such as the guanine radical cation (*24*). After removal of reactive oxygen species, a partner [4Fe4S] protein could then re-reduce Pol δ and restore lagging strand replication. Alternatively, the entire redox cycle could be carried out between Pol δ and other [4Fe4S] proteins associated with the replication fork. The nuclease-helicase Dna2 is a prime example of such a partner, as it associates with the replication fork and is involved in both fork reversal and double strand break repair (*61, 62*). In human cells, the [4Fe4S] DNA repair glycosylase MUTYH associates with PCNA during S-phase; whether this association also occurs in the yeast homologue, Ntg2, is not known (*63*). If the glycosylases do generally associate with the fork, redox signaling could enable rapid communication between replication and repair pathways in eukaryotes. Finally, redox signaling between Pol δ and the B-family translesion DNA synthesis polymerase Pol ζ could help these proteins to hand off DNA containing bulky lesions. Indeed, a role for the cluster in the Pol δ – Pol ζ switch has already been suggested (*64*). In this view, Pol δ and Pol ζ switch by exchanging their shared B-subunits, although this would leave the cluster vulnerable to degradation (*65*). However, a redox handoff similar to that suggested between

primase and Pol α could allow such a transfer without requiring direct subunit exchange (*16*). While redox control of Pol δ would provide clear opportunities and is intriguing to consider, the *in vivo* mechanism and possible partners still require further investigation.

In summary, we have shown that Pol δ can use its [4Fe4S] cluster for reversible electron transfer along DNA and that oxidation of the cluster leads to reversible stalling. Taken together, our data suggest a model in which Pol δ uses redox signaling through DNA to sense oxidative stress, stalling replication under the mutagenic conditions, and potentially coordinating activities with repair and other replication proteins. Overall, the redox sensitivity of Pol δ reveals the oxidation state of the [4Fe4S] cluster to be a critical redox switch, and could provide a means to rapidly and reversibly to respond to replication stress.

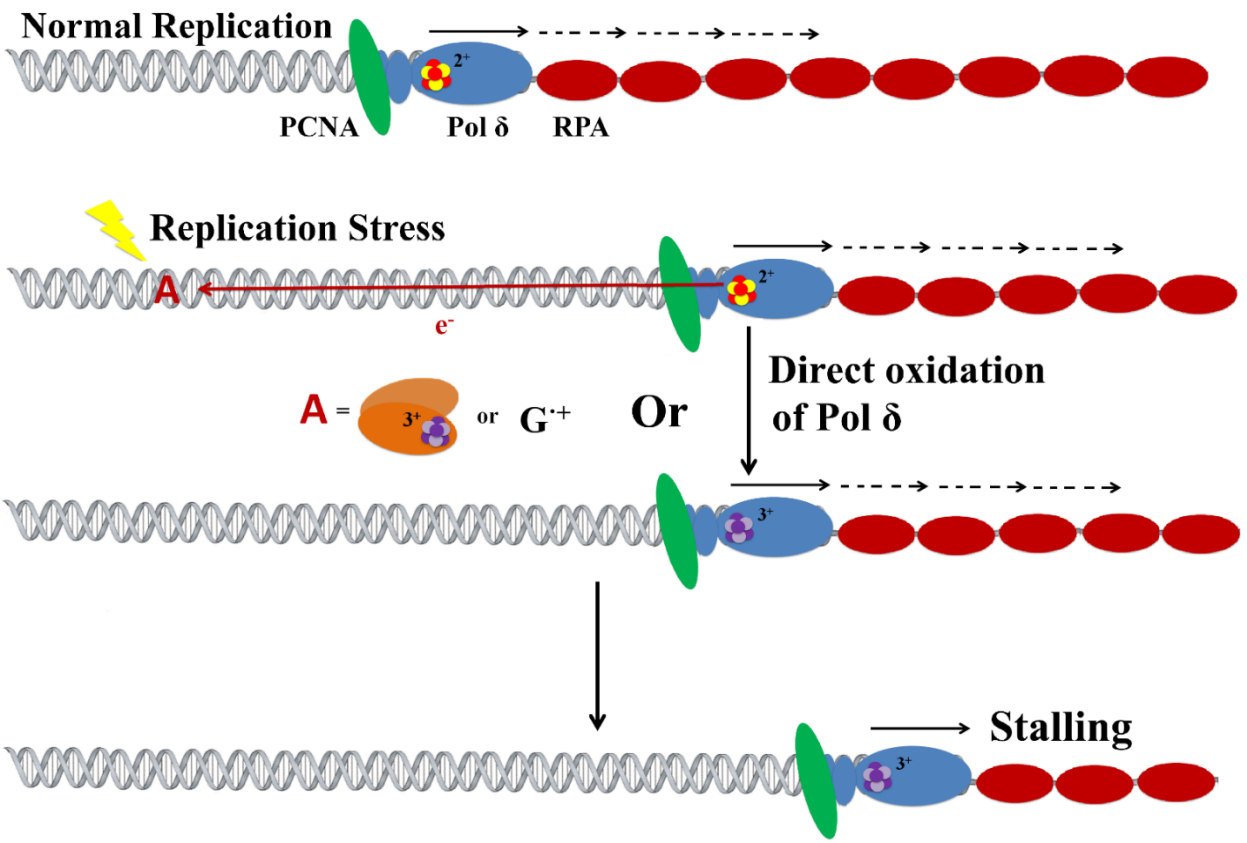

Figure 5.12 A model for redox-mediated regulation of Pol δ activity. Under ordinary circumstances, Pol δ forms a complex with PCNA and processively extends lagging strand DNA (top). When replication stress occurs, lagging strand synthesis could be stalled either by transfer of an electron from the Pol δ $[4Fe4S]^{2+}$ cluster to an acceptor (**A**) or by direct oxidation of the DNA-bound Pol δ-PCNA complex. In the case of DNA-mediated oxidation, the electron acceptor could be an oxidized [4Fe4S] protein or a guanine radical cation, $\mathbf{G}^{\cdot+}$, formed during oxidative stress. Once the cluster is oxidized to the $[4Fe4S]^{3+}$ form, Pol δ binds more tightly to DNA and synthesis slows. After damage resolution, lagging strand replication could be restored by reduction of the $[4Fe4S]^{3+}$ cluster by another [4Fe4S] proteins.

References

1) Lujan, S. A.; Williams, J. S.; Kunkel, T. A. DNA Polymerases Divide the Labor of Genome Replication. *Trends Cell Biol.* **2016**, *26*, 640 – 654.

2) Burgers, P.M.J.; Kunkel, T.A. Eukaryotic DNA Replication Fork. *Annu. Rev. Biochem.* **2017**, *86*, 417 – 438.

3) Johnson, R. E.; Klassen, R.; Prakash, L.; Prakash, S. A Major Role of DNA Polymerase δ in Replication of Both the Leading and Lagging DNA Strands. *Mol. Cell* **2015**, *59*, 163 – 175.

4) Yeeles, J. T. P.; Janska, A.; Early, A.; Diffley, J. F. X. How the Eukaryotic Replisome Achieves Rapid and Efficient DNA Replication. *Mol. Cell* **2017**, *65*, 105 – 116.

5) Prindle, M.J.; Loeb, L.A. DNA Polymerase Delta in DNA Replication and Genome Maintenance. *Environ. Mol. Mutagen.* **2012**, *53*, 666 – 682.

6) Johansson, E.; MacNeill, S. A. The eukaryotic replicative DNA polymerases take shape. *Trends Biochem. Sci.* **2010**, *35*, 339 – 347.

7) Netz, D. J. A.; Stith, C. M.; Stümpfig, M.; Köpf, G.; Vogel, D.; Genau, H. M.; Stodola, J. L.; Lill, R.; Burgers, P. M. J.; Pierik, A. J. Eukaryotic DNA polymerases require an iron-sulfur cluster for the formation of active complexes. *Nat. Chem. Biol.* **2012**, *8*, 125 – 132.

8) Klinge, S.; Núñez-Ramírez, R.; Llorca, O.; Pellegrini, L. 3D architecture of DNA Pol α reveals the functional core of multi-subunit replicative polymerases. *EMBO J.* **2009**, *28*, 1978 – 1987.

9) Netz, D. J. A.; Mascarenhas, J.; Stehling, O.; Pierik, A. J.; Lill, R. Maturation of cytosolic and nuclear iron-sulfur proteins. *Trends Cell Biol.* **2014**, *24*, 303 – 312.

10) Jain, R.; Vanamee, E. S.; Dzikovski, B. G.; Buku, A.; Johnson, R. E.; Prakash, L.; Prakash, S.; Aggarwal, A. K. An Iron-Sulfur Cluster in the Polymerase Domain of Yeast DNA Polymerase ε. *J. Mol. Biol.* **2014**, *426*, 301 – 308.

11) Johnson, D.C.; Dean, D.R.; Smith, A.D.; Johnson, M.K. Structure, Function, and Formation of Biological Iron-Sulfur Clusters. *Annu. Rev. Biochem.* **2005**, *74*, 247 – 281.

12) Swan, M. K.; Johnson, R. E.; Prakash, L.; Prakash, S.; Aggarwal, A. K. Structural basis of high-fidelity DNA synthesis by yeast DNA polymerase delta. *Nat. Struct. Mol. Biol.* **2009**, *16*, 979 – 986.

13) Boal, A. K.; Yavin, E.; Lukianova, O. A.; O'Shea, V. L.; David, S. S.; Barton, J. K. DNA-Bound Redox Activity of DNA Repair Glycosylases Containing [4Fe4S] Clusters. *Biochemistry* **2005**, *44*, 8397 – 8407.

14) Mui, T. P.; Fuss, J. O.; Ishida, J. P.; Tainer, J. A.; Barton, J. K. ATP-Stimulated, DNA-Mediated Redox Signaling by XPD, a DNA Repair and Transcription Helicase. *J. Am. Chem. Soc.* **2011**, *133*, 16378 – 16381.

15) Grodick, M. A.; Segal, H. M.; Zwang, T. J.; Barton, J. K. DNA-Mediated Signaling by Proteins with 4Fe-4S Clusters is Necessary for Genomic Integrity. *J. Am. Chem. Soc.* **2014**, *136*, 6470 – 6478.

16) O'Brien, E.; Holt, M. E.; Thompson, M. K.; Salay, L. E.; Ehlinger, A. C.; Chazin, W. J.; Barton, J. K. The [4Fe4S] cluster of human DNA primase functions as a redox switch using DNA charge transport. *Science* **2017**, *355*, 813.

17) Porello, S. L.; Cannon, M. J.; David, S. S. A Substrate Recognition Role for the [4Fe-4S]$^{2+}$ Cluster of the DNA Repair Glycosylase MutY. *Biochemistry* **1998**, *37*, 6465 – 6475.

18) Fan, L.; Fuss, J. O.; Cheng, Q. J.; Arvai, A. S.; Hammel, M.; Roberts, V. A.; Cooper, P. K.; Tainer, J. A. XPD Helicase Structures and Activities: Insights into the Cancer and Aging Phenotypes from XPD Mutations. *Cell* **2008**, *133*, 789 – 800.

19) Ren, B.; Duan, X.; Ding, H. Redox control of the DNA damage-inducible protein DinG helicase activity via its iron-sulfur cluster. *J. Biol. Chem.* **2009**, *284*, 4829 – 4835.

20) Weiner, B. E.; Huang, H.; Dattilo, B. M.; Nilges, M. J.; Fanning, E.; Chazin, W. J. An Iron-Sulfur Cluster in the C-terminal Domain of the p58 Subunit of Human DNA Primase. *J. Biol. Chem.* **2007**, *282*, 33444 – 33451.

21) Gorodetsky, A.A.; Boal, A.K.; Barton, J.K. Direct Electrochemistry of Endonuclease III in the Presence and Absence of DNA. *J. Am. Chem. Soc.* **2006**, *128*, 12082 – 12083.

22) Bartels, P.L.; Zhou, A.; Arnold, A.R.; Nuñez, N.N.; Crespilho, F.N.; David, S.S.; Barton, J.K. Electrochemistry of the [4Fe4S] Cluster in Base Excision Repair Proteins: Tuning the Redox Potential with DNA. *Langmuir* **2017**, *33*, 2523 – 2530.

23) Ha, Y.; Arnold, A.R.; Nuñez, N.N.; Bartels, P.L.; Zhou, A.; David, S.S.; Barton, J.K.; Hedman, B.; Hodgson, K.O.; Solomon, E.I. Sulfur K-Edge XAS Studies of the Effect of DNA Binding on the [Fe_4S_4] Site in EndoIII and MutY. *J. Am. Chem. Soc.* **2017**, *139*, 11434 – 11442.

24) Yavin, E.; Boal, A. K.; Stemp, E. D. A.; Boon, E. M.; Livingston, A. L.; O'Shea, V. L.; David, S. S.; Barton, J. K. Protein-DNA Charge Transport: Redox Activation of a DNA Repair Protein by Guanine Radical. *Proc. Natl. Acad. Sci. U. S. A.* **2005**, *102*, 3546 – 3551.

25) Dey, A.; Jenney, F. E.; Adams, M. W. W.; Babini, E.; Takahashi, Y.; Fukuyama, K.; Hodgson, K. O.; Hedman, B.; Solomon, E. I. Solvent Tuning of Electrochemical Potentials in the Active Sites of HiPIP vs Ferredoxin. *Science* **2007**, *318*, 1464 – 1468.

26) Arnold, A. R.; Grodick, M. A.; Barton, J. K. DNA Charge Transport: from Chemical Principles to the Cell. *Cell Chem. Biol*. **2016**, *23*, 183 – 197.

27) Tse, E.C.M.; Zwang, T.J.; Barton, J.K. The Oxidation State of [4Fe4S] Clusters Modulates the DNA-Binding Affinity of DNA Repair Proteins. *J. Am. Chem. Soc.* **2017**, *139*, 12784 – 12792.

28) Pheeney, C. G.; Arnold, A. R.; Grodick, M. A.; Barton, J. K. Multiplexed Electrochemistry of DNA-Bound Metalloproteins. *J. Am. Chem. Soc.* **2013**, *135*, 11869 – 11878.

29) Slinker, J. D.; Muren, N. B.; Gorodetsky, A.A.; Barton, J. K. Multiplexed DNA-Modified Electrodes. *J. Amer. Chem. Soc.* **2010**, *132*, 2769 – 2774.

30) Barton, J.K.; Bartels, P.L.; Deng, Y.; O'Brien, E. Electrical Probes of DNA-Binding Proteins. *Methods Enzymol.* **2017**, *591*, 355 – 414.

31) Greeley, R. S.; Smith, W. T.; Stoughton, R. W.; Lietzke, M. H. Electromotive Forces in Aqueous Solutions at Elevated Temperatures. I. The Standard Potential of the Silver-Silver Chloride Electrode. *J. Phys. Chem.* **1960**, *64*, 652 – 657.

32) Burgers, P. M. J.; Yoder, B. L. ATP-Independent Loading of the Proliferating Cell Nuclear Antigen Requres DNA Ends. *J. Biol. Chem.* **1993**, *268*, 19923 – 19926.

33) Garg, P.; Stith, C. M.; Sabouri, N.; Johansson, E.; Burgers, P. M. Idling by DNA polymerase δ maintains a ligatable nick during lagging-strand DNA replication. *Genes Dev.* **2004**, *18*, 2764 – 2773.

34) Kissinger, P. T.; Heineman, W. R. Large-Amplitude Controlled-Potential Techniques in *Laboratory Techniques in Electroanalytical Chemistry*, *2nd ed.* (Kissinger, P.T. and Heineman, W.R., eds.), **1996**, pp. 51 – 139, Marcel Dekker, New York.

35) Stodola, J.L.; Burgers, P.M. Resolving individual steps of Okazaki-fragment maturation at a millisecond time scale. *Nat. Struct. Mol. Biol.* **2016**, *23*, 402 – 408.

36) Schaefer, K. N.; Barton, J. K. DNA-Mediated Oxidation of p53. *Biochemistry* **2014**, *53*, 3467 – 3475.

37) Johnson, R. E.; Prakash, L.; Prakash, S. Yeast and Human Translesion DNA Synthesis Polymerases: Expression, Purification, and Biochemical Characterization. *Methods Enzymol*. **2006**, *408*, 390 – 407.

38) Tomoaki, O.; Nakamura, H., Katsumi, N.; Cusanovich, M.A.; Akutsu, H. Ionic Strength-Dependent Physicochemical Factors in Cytochrome c_3 Regulating the Electron Transfer Rate. *Biophys. J.* **1998**, *75*, 1483 – 1490.

39) Lode, E.T.; Murray, C.L.; Rabinowitz, J.C. Apparent oxidation-reduction potential of *Clostridium acidiurici* ferredoxin. Effect of pH, ionic strength, and amino acid replacements. *J. Biol. Chem.* **1976**, *251*, 1683 – 1687.

40) Johansson, E.; Majka, J.; Burgers, P.M. Structure of DNA Polymerase δ from *Saccharomyces cerevisiae*. *J. Biol. Chem.* **2001**, *276*, 43824 – 43828.

41) Boon, E. M.; Salas, J. E.; Barton, J. K. An Electrical Probe of Protein-DNA Interactions On DNA-Modified Surfaces. *Nat. Biotechnol.* **2002**, *20*, 282 – 286.

42) Kelley, S. O.; Barton, J. K.; Jackson, N. M.; Hill, M. G. Electrochemistry of Methylene Blue bound to a DNA-Modified Electrode. *Bioconjug. Chem.* **1997**, *8*, 31 – 37.

43) Sweeney, W. V; Rabinowitz, J. C. Proteins Containing 4Fe-4S Clusters: An Overview. *Annu. Rev. Biochem.* **1980**, *49*, 139 – 161.

44) Johnson, M. K.; Duderstadt, R. E.; Duin, E. C. Biological and Synthetic $[Fe_3S_4]$ Clusters. *Adv. Inorg. Chem.* **1999**, *47*, 1 – 82.

45) Duff, J. L. C.; Breton, J. L. J.; Butt, J. N.; Armstrong, F. A.; Thomson, A. J. Novel Redox Chemistry of [3Fe-4S] Clusters: Electrochemical Characterization of the All-Fe(II) Form of the [3Fe-4S] Cluster Generated Reversibly in Various Proteins and Its Spectroscopic Investigation in *Sulfolobus acidocaldarius* Ferredoxin. *J. Am. Chem. Soc.* **1996**, *118*, 8593 – 8603.

46) Hedglin, M.; Pandey, B.; Benkovic, S. J. Stability of the human polymerase δ holoenzyme and its implications in lagging strand DNA synthesis. *Proc. Natl. Acad. Sci.* **2016**, *13*, E1777 – 1786.

47) Kulak, N.A.; Pichler, G.; Paron, I.; Nagaraj, N.; Mann, M. Minimal, encapsulated proteomic-sample processing applied to copy-number estimation in yeast. *Nat. Methods* **2014**, *11*, 319 – 324.

48) Goffeau, A.; Barrell, B.G.; Bussey, H.; Davis, R.W.; Dujon, B.; Feldmann, H.; Galibert, F.; Hoheisel, J.D.; Jacq, C.; Johnston, M.; Louis, E.J.; Mewes, H.W.; Murakami, Y.; Philippsen, P.; Tettelin, H.; Oliver, S.G. A Gene Map of the Human Genome. *Science* **1996**, *274*, 546 – 567.

49) Lengronne, A.; Pasero, P.; Bensimon, A.; Schwob, E. Monitoring S phase progression globally and locally using BrdU incorporation in TK^+ yeast strains. *Nucleic Acids Res.* **2001**, *29*, 1433 – 1422.

50) Henderson, P.T.; Jones, D.; Hampikian, G.; Kan, Y.; Schuster, G.B. Long-distance charge transport in duplex DNA: The phonon-assisted polaron-like hopping mechanism. *Proc. Natl. Acad. Sci. U.S.A.* **1999**, *96*, 8353 – 8358.

51) Armitage, B.; Yu, C.; Devadoss, C.; Schuster, G.B. Cationic Anthraquinone Derivatives as Catalytic DNA Photonucleases: Mechanisms for DNA Damage and Quinone Recycling. *J. Am. Chem. Soc.* **1994**, *116*, 9847 – 9859.

52) Gasper, S.M.; Schuster, G.B. Intramolecular Photoinduced Electron Transfer to Anthraquinones Linked to Duplex DNA: The Effect of Gaps and Traps on Long-Range Radical Cation Migration. *J. Am. Chem. Soc.* **1997**, *119*, 12762 – 12771.

53) Nuñez, M.E.; Hall, D.B.; Barton, J.K. Oxidative Charge Transport through DNA in Nucleosome Particles. *Chem. Biol.* **1999**, *6*, 85 – 97.

54) Berti, M.; Vindigni, A. Replication stress: getting back on track. *Nat. Struct. Mol. Biol.* **2016**, *23*, 103 – 109.

55) De Piccoli, G.; Katou, Y.; Itoh, T.; Nakato, R.; Shirahige, K.; Labib, K. Replisome stability at defective DNA replication forks is independent of S-phase checkpoint kinases. *Mol. Cell.* **2012**, *45*, 696 – 704.

56) Zeman, M.K.; Cimprich, K.A. Causes and consequences of replications stress. *Nat. Cell Biol.* **2014**, *16*, 2 – 9.

57) Saldivar, J.C.; Cortez, D.; Cimprich, K.A. The essential kinase ATR: ensuring faithful duplication of a challenging genome. *Nat. Rev. Mol. Cell Biol.* **2017**, *18*, 622 – 636.

58) Azzam, E.I.; Jay-Gerin, J.P.; Pain, D. Ionizing radiation-induced metabolic oxidative stress and prolonged cell injury. *Cancer Lett.* **2012**, *327*, 48 – 60.

59) McCulloch, S.D.; Kokoska, R.J.; Garg, P.; Burgers, P.M.; Kunkel, T.A. The efficiency and fidelity of 8-oxo-guanine bypass by DNA polymerases δ and η. *Nucleic Acids Res.* **2009**, *37*, 2830 – 2840.

60) Zellweger, R.; Dalcher, D.; Mutreja, K.; Berti, M.; Schmid, J. A.; Herrador, R.; Vindigni, A.; Lopes, M. Rad51-Mediated Fork Reversal is a Global Response to Genotoxic Treatments in Human Cells. *J. Cell Biol.* **2015**, *208*, 563 – 579.

61) Thangavel, S.; Berti, M.; Levikova, M.; Pinto, C.; Gomathinayagam, S.; Vujanovic, M.; Zellweger, R.; Moore, H.; Lee, E. H.; Hendrickson, E. A.; Cejka, P.; Stewart, S.; Lopes, M.; Vindigni, A. DNA2 Drives Processing and Restart of Reversed Replication Forks in Human Cells. *J. Cell Biol.* **2015**, *208*, 545 – 562.

62) Nimonkar, A. V.; Genschel, J.; Kinoshita, E.; Polaczek, P.; Campbell, J. L.; Wyman, C.; Mdrich, P.; Kowalczykowski, S. C. BLM-DNA2-RPA-MRN and EXO1-BLM-RPA-

MRN constitute two DNA end resection machineries for human DNA break repair. *Genes Dev.* **2011**, *25*, 350 – 362.

63) Markkanen, E.; Dorn, J.; Hübscher, U. MUTYH DNA glycosylase: the rationale for removing undamaged bases from the DNA. *Front. Genet.* **2013**, *4*, 18.

64) Baranovskiy, A. G.; Lada, A. G.; Siebler, H. M.; Zhang, Y.; Pavlov, Y. I.; Tahirov, T. H. DNA polymerase δ and ζ switch by sharing accessory subunits of DNA polymerase δ. *J. Biol. Chem.* **2012**, *287*, 17281 – 17287.

65) Johnson, R. E.; Prakash, L.; Prakash, S. Pol31 and Pol32 subunits of yeast DNA polymerase δ are also essential subunits of DNA polymerase ζ. *Proc. Natl. Acad. Sci. U. S. A.* **2012**, *109*, 12455 – 12460.